Propagation of High-Energy 10.6-Micron Laser Beams Through the Atmosphere

ALFRED H. AITKEN

Theory Branch
Nuclear Physics Division

JOHN N. HAYES
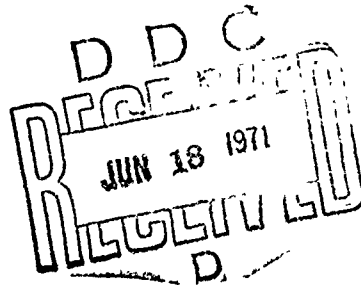
Applied Optics Branch
Optical Sciences Division

and

PETER B. ULRICH

Analysis Staff
Optical Sciences Division

May 28, 1971

NAVAL RESEARCH LABORATORY
Washington, D.C.

DOCUMENT CONTROL DATA - R & D

(Security classification of title, body of abstract and indexing annotation must be entered when the overall report is classified)

1 ORIGINATING ACTIVITY (Corporate author)	2a. REPORT SECURITY CLASSIFICATION
Naval Research Laboratory Washington, D.C. 20390	Unclassified
	2b GROUP

3 REPORT TITLE

PROPAGATION OF HIGH-ENERGY 10.6-MICRON LASER BEAMS THROUGH THE ATMOSPHERE

4 DESCRIPTIVE NOTES (Type of report and inclusive dates)

This is an interim report on a continuing problem.

5 AUTHOR(S) (First name, middle initial, last name)

Alfred H. Aitken, John N. Hayes, and Peter B. Ulrich

6 REPORT DATE	7a. TOTAL NO OF PAGES	7b NO OF REFS
May 28, 1971	46	19

8a. CONTRACT OR GRANT NO	9a. ORIGINATOR'S REPORT NUMBER(S)
NRL Problems R05-31.304 and N01-23.101	NRL Report 7293
b PROJECT NO ORD 0832-129-17ᵤ-1, Task U1754-2	
c.	9b OTHER REPORT NO(S) (Any other numbers that may be assigned this report)
d.	

10 DISTRIBUTION STATEMENT

Approved for public release; distribution unlimited.

11 SUPPLEMENTARY NOTES	12 SPONSORING MILITARY ACTIVITY
	Dept. of the Navy (Naval Ordnance Systems Command), Washington, D.C. 20360

13 ABSTRACT

The purpose of the present investigation is the determination of the properties of an intense 10.6-micron laser beam propagating through the open atmosphere in the presence of wind or slewing, or both. It is shown that the Maxwell equations can, in this problem, be reduced to the study of the scalar wave equation with a varying index of refraction. The index of refraction is related to the atmospheric density; therefore, the density changes in the air due to beam absorption are related to the absorption coefficient of the air and to the intensity of the beam, using the linearized hydrodynamic equations. A detailed discussion of the mechanisms of photon absorption by the constituents of the air is presented. The resultant equation for the scalar wave is a nonlinear partial differential integral equation which is solved numerically. The algorithm used for the computer code is discussed, together with criteria that have been determined to be useful in assessing the accuracy and reliability of the numerical results. The solutions of several different problems are presented and discussed. In particular, it is found that (a) beam quality is degraded for water vapor pressures at or near sea level, and (b) beam slewing reduces the detrimental effect of water vapor.

14 KEY WORDS	LINK A		LINK B		LINK C	
	ROLE	WT	ROLE	WT	ROLE	WT
Laser beams						
Propagation						
Atmosphere						
Light transmission						
Interaction with matter						
Nonlinear optics						
Thermal blooming						

CONTENTS

ABSTRACT

The purpose of the present investigation is the determination of the properties of an intense 10.6-micron laser beam propagating through the open atmosphere in the presence of wind or slewing, or both. It is shown that the Maxwell equations can, in this problem, be reduced to the study of the scalar wave equation with a varying index of refraction. The index of refraction is related to the atmospheric density; therefore, the density changes in the air due to beam absorption are related to the absorption coefficient of the air and to the intensity of the beam, using the linearized hydrodynamic equations. A detailed discussion of the mechanisms of photon absorption by the constituents of the air is presented. The resultant equation for the scalar wave is a nonlinear partial differential integral equation which is solved numerically. The algorithm used for the computer code is discussed, together with criteria that have been determined to be useful in assessing the accuracy and reliability of the numerical results. The solutions of several different problems are presented and discussed. In particular, it is found that (a) beam quality is degraded for water vapor pressures at or near sea level, and (b) beam slewing reduces the detrimental effect of water vapor.

PROBLEM STATUS

This is an interim report on a continuing problem.

AUTHORIZATION

PROPAGATION OF HIGH-ENERGY 10.6-MICRON LASER BEAMS THROUGH THE ATMOSPHERE

I. INTRODUCTION

The development of the gas dynamic laser has turned the prospect of a cw high-power laser into a reality. Many applications of these devices involve propagation of the beam through the atmosphere, and thus an understanding of the various aspects of beam-atmosphere interactions is required. This report is devoted to a study of one of the non-linear aspects of the propagation of laser radiation through air, namely, the change due to absorption of beam energy in the index of refraction of the air, which in turn modifies the propagation of the beam. Beam energy absorption by an otherwise motionless atmosphere induces temperature changes in the medium, which in turn cause a defocusing (or focusing) of the beam that changes with time. A number of studies have been made of this phenomenon, which is often referred to as thermal blooming (1-7).

If a steady wind is present with a nonzero component transverse to the beam axis, the heated air is swept out of the beam and a steady-state ultimately evolves (8). Beam slewing under suitable conditions likewise gives rise to a steady state. The formulation and description of these steady states is the problem this report addresses. The existence and stability of such states is assumed. Theoretical and experimental studies of cases such as these have been made (9).

Section II of this report presents the formulation of the physical assumptions of the problem. Section III is a discussion of the techniques used in a numerical solution of the equations derived in Section II, while Section IV is a discussion of the results of several numerical solutions, and a presentation of the basic limitations of the algorithm used to obtain the numerical solutions.

II. FORMULATION OF THE PROBLEM

Outline

An equation which contains the index of refraction of the air is developed to describe the propagation of the laser beam. The index and the density of the air are related by the Lorentz-Lorenz law. The air density is in turn related to the heat sources in the air that arise from beam absorption through the linearized hydrodynamic equations. Finally, a detailed discussion of the mechanism of absorption of 10.6-micron radiation along the lines developed by Wood, Camac, and Gerry (10) is included.

Propagation Equation

The wave equation for a harmonically varying electric field in a medium of varying dielectric coefficient is

$$\nabla^2 \mathbf{E} + k^2 \epsilon \mathbf{E} = \vec{\nabla}\vec{\nabla} \cdot \mathbf{E}$$

with $k = \omega/c$, where ω is the angular frequency, and ϵ is the dielectric coefficient. Using the equation of charge conservation, the divergence term on the right-hand side is given by

$$\vec{\nabla} \cdot \vec{E} = - \epsilon^{-1} \vec{E} \cdot \vec{\nabla}\epsilon \quad .$$

If the properties of the medium are such that variations of the dielectric coefficient are small in a wavelength, the right-hand term may be neglected in comparison with the $k^2\epsilon E$ term in the first equation, yielding simply

$$\nabla^2 E + k^2\epsilon E = 0 \quad .$$

This approximation also implies that the polarization of the field is not changed as it propagates so that only linearly polarized amplitudes need be considered. Further, since the principal concern is with a beam which in the first approximation is simply propagating along the z axis, a solution of the form $E = \hat{e}\varphi(r)\, \exp(ik\sqrt{\epsilon_0}\, z)$ is anticipated, where φ is assumed to be a slowly varying function of z, ϵ_0 is the dielectric constant of the medium prior to its interaction with the beam, and $\hat{e}$ is a unit vector transverse to the beam axis. ϵ and ϵ_0 each have an imaginary part that describes beam absorption; because density changes will be small, $\epsilon^{(i)} = \epsilon_0^{(i)}$ to an excellent approximation. Therefore, the equation for φ is

$$\frac{\partial^2\varphi}{\partial z^2} + 2ik\,\frac{\partial\varphi}{\partial z} + \nabla_\perp^2\varphi + k^2(\epsilon^{(r)} - \epsilon_0^{(r)})\varphi = 0$$

where $\nabla_\perp^2 = \partial^2/\partial x^2 + \partial^2/\partial y^2$. In accord with the expectation that φ be a slowly varying function of z, the second-derivative term is dropped as being small compared with the first-derivative term. The equation that describes the laser beam then is

$$2ik\,\frac{\partial\varphi}{\partial z} + \nabla_\perp^2\varphi + k^2(\epsilon^{(r)} - \epsilon_0^{(r)})\varphi = 0 \quad . \tag{1}$$

Equation (1), being essentially a two-dimensional Schrödinger equation with z playing the role of time, has the quantity

$$\iint_{z=\text{constant}} \varphi^*(x,y,z)\, \varphi(x,y,z)\, dx\, dy \tag{2}$$

as a constant of the motion.

The energy flux is described by the time-averaged Poynting vector. With the approximations described above included in the standard expression for the Poynting vector, the energy flux becomes

$$P = \frac{c}{8\pi}\, e^{-\alpha z}\, \varphi^*\varphi\, \hat{e}_z \tag{3}$$

where $\alpha = 2\epsilon_0^{(i)}$. The total power P passing through a plane $z = $ constant is given by

$$P(z) = \frac{c}{8\pi}\, e^{-\alpha z} \iint_{z=\text{constant}} dx\, dy\, \varphi^*\varphi \quad . \tag{4}$$

$\hat{e}_z$ is unit vector along z axis. Equation (1), supplemented with a relationship between the dielectric constant $\epsilon^{(r)}$ and the function φ, is the equation to be solved.

Hydrodynamics

The atmosphere will be treated as a perfect fluid; viscous and thermal conduction effects will be ignored since their consequences can be shown to be negligible in the cases that will be considered in this paper. The beam will be regarded as an external heat source described by an energy deposition function $\dot{Q}$, representing the energy deposited per gram per second at each point in the fluid. A complete description of the hydrodynamic system is thus provided by the boundary conditions, the equation of state, an expression for the internal energy of the fluid, and the hydrodynamic equations of motion:

$$\frac{d\rho}{dt} + \rho \vec{\nabla} \cdot \mathbf{v} = 0 ,$$

$$\rho \frac{d\mathbf{v}}{dt} + \vec{\nabla} p = 0 ,$$

$$\rho \frac{d\mathcal{E}}{dt} + p \nabla \cdot \mathbf{v} = \rho \dot{Q}$$

$$\mathcal{E} = c_v T ,$$

$$\frac{p}{\rho} = (c_p - c_v) T .$$

The quantities ρ, $\mathbf{v}$, p, $\mathcal{E}$, T, c_v, and c_p represent the density, fluid velocity, pressure, internal energy per unit mass, temperature, specific heat at constant volume, and specific heat at constant pressure, respectively. The operator d/dt stands for the substantial derivative.

During the course of fluid motion through the laser beam, the temperature change of a fluid element will, in most circumstances, be small so that the specific heats may be regarded as constant throughout the flow. Under these conditions, the first, third, fourth, and fifth of these equations may be combined to yield an expression involving pressure and density alone:

$$\frac{dp}{dt} - \gamma \frac{p}{\rho} \frac{d\rho}{dt} = (\gamma - 1) \rho \dot{Q}$$

where $\gamma = c_p/c_v$. Further, because the changes in the pressure, density, and velocity are expected to be small, the linearized hydrodynamic equations can be regarded as a good description of the physical system. Let the pressure p_0, density ρ_0, and velocity v_0 of the fluid satisfy the unperturbed exact hydrodynamic equations

$$\frac{d\rho_0}{dt} + \rho_0 \vec{\nabla} \cdot \mathbf{v}_0 = 0 ,$$

$$\rho_0 \frac{d\mathbf{v}_0}{dt} + \vec{\nabla} p_0 = 0 ,$$

$$\frac{d\rho_0}{dt} - \gamma \frac{p_0}{\rho_0} \frac{dp_0}{dt} = 0 .$$

The total pressure, density, and velocity are taken to be

$$p = p_0 + p_1 \quad ,$$

$$\rho = \rho_0 + \rho_1 \quad ,$$

$$v = v_0 + v_1 \quad .$$

The subscripted quantities p_1, ρ_1, and v_1 are taken to be of the first order, and higher powers of these terms are deemed negligible. Particularizing to the case of a beam in the presence of a steady uniform wind ($v_0 =$ constant), the first-order quantities are taken to satisfy the equations

$$\frac{d\rho_1}{dt} + \rho_0 \vec{\nabla} \cdot v_1 = 0 \tag{5}$$

$$\rho_0 \frac{dv_1}{dt} + \vec{\nabla} p_1 = 0 \tag{6}$$

$$\frac{dp_1}{dt} - \gamma \frac{\rho_0}{\rho_0} \frac{d\rho_1}{dt} = (\gamma - 1) \, \rho_0 \dot{Q} \tag{7}$$

where, *now*, the operator d/dt is taken to be

$$\frac{d}{dt} = \frac{\partial}{\partial t} + v_0 \cdot \vec{\nabla} \quad . \tag{8}$$

The term $\gamma p_0 / \rho_0$ is c_s^2, where c_s is the speed of sound in the fluid prior to the perturbations caused by the beam.

Since the steady-state case is the solution of interest, the hydrodynamic quantities at a fixed point in space are taken to be independent of time. Therefore all partial time derivatives of these quantities vanish, and the equations of motion reduce to

$$v_0 \cdot \vec{\nabla} \rho_1 + \rho_0 \vec{\nabla} \cdot v_1 = 0 \quad , \tag{9}$$

$$\rho_0 v_0 \cdot \vec{\nabla} v_1 + \vec{\nabla} p_1 = 0 \quad , \tag{10}$$

$$v_0 \cdot \vec{\nabla} \, (p_1 - c_s^2 \rho_1) = (\gamma - 1) \, \rho_0 \dot{Q} \quad . \tag{11}$$

The last equation may be integrated to give

$$\rho_1 = - \frac{(\gamma - 1)}{v_0 c_s^2} \int_{-\infty}^{0} ds \, \rho_0 \dot{Q} (r + s \hat{v}_0) + \frac{p_1}{c_s^2} \tag{12}$$

where $\hat{v}_0$ is a unit vector along the direction of the wind velocity and the integral is along the path of motion of a fluid element. The path is parameterized by the path length s which is taken to be zero when the fluid element is at the point r. By elimination of the density and velocity in favor of the pressure, a differential equation for the pressure change alone is easily obtained:

$$\left[\nabla^2 - \left(\frac{v_0 \vec{\nabla}}{c_s} \right)^2 \right] p_1 = - \frac{(\gamma - 1)}{c_s^2} v_0 \cdot \vec{\nabla} \, \rho_0 \dot{Q} \tag{13}$$

An estimate of the contribution of the pressure term to the density can be obtained by ignoring the pressure gradient along the beam axis and the gradient perpendicular to the wind velocity; then

$$p_1(r) \simeq - \frac{(\gamma - 1) v_0}{\left(1 - \frac{v_0^2}{c_s^2} \right) c_s^2} \int_{-\infty}^{0} ds \, \rho_0 \dot{Q} \, (r + s \hat{v}_0) \quad . \tag{14}$$

Restricting wind speeds to values much smaller than the speed of sound, the pressure term may clearly be ignored, and the density change of air at any point r is given by

$$\rho_1(r) = - \frac{(\gamma - 1)}{v_0 c_s^2} \int_{-\infty}^{0} ds \, \rho_0 \dot{Q} (r + s \hat{v}_0) \quad . \tag{15}$$

Equation (15) shows clearly that a zero wind speed is not tenable in this treatment; a steady state cannot be achieved without the wind as a mechanism for removing the heated air from the beam. Furthermore, Eq. (15) can be used as a means for estimating the limits that must be placed upon the beam intensity, wind velocity, and absorption coefficient for the linearized treatment used here to retain its validity. If beam absorption leads instantaneously to heating, then the quantity $\rho_0 \dot{Q}$ becomes αI, where I is the beam intensity. The integral may be approximated by $2\alpha \bar{I} a$ where $\bar{I}$ is an average power distribution along a line across the laser face through the center, and a is the beam radius. Then, if the density change must be less than $\hat{\rho}_1$ to preserve the validity of the linearization of the hydrodynamic equations, $\bar{I}$, α, and v_0 must together satisfy the inequality

$$\left| \frac{\alpha \bar{I} a}{v_0} \right| \le \frac{\hat{\rho}_1 c_s^2}{2(\gamma - 1)} \quad . \tag{16}$$

In this formulation of the propagation of a laser beam in the presence of a steady wind, there exists a reflection symmetry in the fluid variables and the beam intensity through a plane encompassing the beam axis and a line parallel to the wind velocity. This symmetry has considerable utility in the numerical solution of the problem.

Important applications may be envisaged wherein the laser beam is required to rotate about an axis perpendicular to the beam axis; such motion, referred to henceforth as beam slewing, can be brought within the framework of a steady-state calculation similar to the discussion above. Beam slewing in an otherwise stationary atmosphere will not lead to a steady state, in part because there is no mechanism for removing the heated air in the vicinity of the laser face, even though the slewing does so further downrange. Therefore, the initial conditions will be functions of time. A steady state can be achieved by the introduction of a mechanism for removing the heated air from the vicinity of the face of the laser; such a mechanism may be modeled in a wide variety of ways, three of which will be briefly discussed here.

In a coordinate system rotating with the laser, the hydrodynamic equations assume the form

$$\left(\frac{\partial}{\partial t} + v \cdot \vec{\nabla} \right) \rho = - \rho \vec{\nabla} \cdot v \tag{17}$$

AITKEN, HAYES, AND ULRICH

$$\left(\frac{\partial}{\partial t} + \mathbf{v} \cdot \vec{\nabla}\right)\mathbf{v} = -\frac{1}{\rho}\vec{\nabla}p - 2\Omega \times \mathbf{v} - \Omega \times (\Omega \times \mathbf{r}) \tag{18}$$

$$\left(\frac{\partial}{\partial t} + \mathbf{v} \cdot \vec{\nabla}\right)p = \frac{\gamma p}{\rho}\left(\frac{\partial}{\partial t} + \mathbf{v} \cdot \vec{\nabla}\right)\rho + (\gamma - 1)\rho\dot{Q} \tag{19}$$

where $\mathbf{v}$ is the fluid velocity measured relative to the rotating reference frame, p and ρ represent the pressure and density, respectively, while Ω is the angular slewing rate, which is orthogonal to the beam direction. These equations, when linearized, assume the forms, for the steady state,

$$(\mathbf{v}_0 \cdot \vec{\nabla})\rho_1 = -\rho_0\vec{\nabla} \cdot \mathbf{v}_1 \tag{20}$$

$$(\mathbf{v} \cdot \vec{\nabla})\mathbf{v}_1 + \Omega \times \mathbf{v}_1 = -\frac{1}{\rho_0}\vec{\nabla}p_1 \tag{21}$$

$$(\mathbf{v}_0 \cdot \vec{\nabla})\,(p_1 - c_s^2\rho_1) = (\gamma - 1)\rho_0\dot{Q} \tag{22}$$

while the zeroth-order quantities satisfy equations of the form of Eqs. (17)-(19) with the heating term dropped. An exact solution of the (nonlinear) zeroth-order equations is provided by

$$\mathbf{v}_0 = \mathbf{w}_0 - \Omega \times \mathbf{r} \tag{23}$$

where $\mathbf{w}_0$ is a velocity vector parallel to Ω. For nonvanishing $\mathbf{w}_0$, this solution corresponds to a wind along the slewing axis, and this wind serves as a mechanism for removing the heated air from the laser face. In the rotating coordinate system, a fluid particle is moving in a spiral path about the slewing axis, and its trajectory is given by

$$\mathbf{r}(s) = \left(x_0 \frac{w_0}{v_0}\, s\right)\mathbf{i} + \left(y_0 \cos\frac{\Omega s}{v_0} + z_0 \sin\frac{\Omega s}{v_0}\right)\mathbf{j}$$

$$+ \left(-y_0 \sin\frac{\Omega s}{v_0} + z_0 \cos\frac{\Omega s}{v_0}\right)\mathbf{k} \tag{24}$$

while the magnitude of the fluid velocity is $\left(w_0^2 + \Omega^2 z^2\right)^{1/2}$ and is a constant for a given fluid element. Under these conditions, Eq. (22) may be integrated to give

$$\rho_1(\mathbf{r}(s)) = -\frac{(\gamma - 1)}{v_0 c_s^2}\int_0^s ds'\rho_0\dot{Q}(\mathbf{r}(s')) + \frac{p_1(\mathbf{r}(s))}{c_s^2}$$

$$+ \left[\rho_1(\mathbf{r}_0) - \frac{p_1(\mathbf{r}_0)}{c_s^2}\right]. \tag{25}$$

The point $\mathbf{r}_0$ may be chosen to represent a point in space where the beam has not arrived, so that the density and pressure changes there vanish; hence the factor in brackets in Eq. (25) may be set equal to zero. An expression for the pressure change alone may be derived in much the same manner as before. Again, the contributions of the pressure term can be shown to be negligible provided that $v_0 < c_s$; however, with slewing present, v_0 can become quite large for long distances down the beam. Therefore, the linearization of the hydrodynamic equations will be valid only for restricted

distances z_M downbeam for which $z_M \ll c_s/\Omega$. Within these limitations, the solution for the density change is given by

$$\rho_1(\mathbf{r}) = -\frac{(\gamma - 1)}{v_0 c_s^2} \int_0^s ds' \, \rho_0 \dot{Q}(\mathbf{r}(s')) \ . \tag{26}$$

$$v_0 = \left(w_0^2 + \Omega^2 z^2\right)^{1/2} \ . \tag{27}$$

On the basis of the above solution, three models can be described.

1. The velocity component w_0 is nonvanishing. As previously mentioned, a wind of this type serves as a device for removing the heated air from the laser face, allowing a steady state to be achieved, and permits an arbitrary number of rotations of the laser about its slewing axis. This solution has the disadvantage that the symmetry described at the end of the formulation of the steady-wind solution is lost, and therefore doubles the computational effort in a numerical solution of the problem.

2. Set the velocity component $w_0 = 0$, and do not allow the axis of revolution to go through the laser face, but instead let it be at a distance D behind it. Then the rotation itself removes the heated air from the laser face; all that is required is that the steady state set in prior to one complete rotation of the laser about the slewing axis. If a distance R down the beam axis is measured in terms of z, the distance from the laser face, then

$$v_0 = \Omega(D + z)$$

$$= v_0' + \Omega z \ . \tag{28}$$

This method has the advantage, from the standpoint of numerical computation, of preserving the symmetry that reduces computation times.

3. Again, set the velocity component $w_0 = 0$; in the rotating reference frame, rigidly attached to the laser, set up a fan that blows air at a velocity v_0' at right angles to the beam axis and the slewing axis, in addition to the slewing velocity, for a fixed distance D down the beam axis. Then v_0 in Eq. (27) is replaced by

$$v_0 = \begin{Bmatrix} v_0' + \Omega z \ , & 0 < z < D \\ \Omega z & , & D < z \end{Bmatrix} \tag{29}$$

which, in for $\dots$, is similar to the second model for slewing. This model also preserves the desired symmetry.

The model used in calculations here will be the second model. All three models admit a new parameter, in addition to the slewing rate Ω; solutions will therefore be dependent upon the value of the parameter. This parameter dependence is expected to be discernible, but not of vital importance.

Absorption of 10.6-Micron Radiation By Air; Kinetic Cooling

The constituents of air that are the principal absorbers of 10.6-micron radiation are water vapor and carbon dioxide. Pressure broadened levels of water vapor make it an effective absorber of infrared radiation throughout a broad band that includes 10.6 microns, while carbon dioxide absorbs principally through the inverse laser transition. These processes have been briefly discussed by Wood, Camac, and Gerry (10) and have been applied in a study of CO_2 laser propagation in geometrical optics by Wallace and Camac (11). Because of its importance to the character of the results, a detailed discussion of the absorption mechanism is presented here.

Water molecules, upon absorption of one photon of 10.6-micron radiation, are excited to the (010) vibrational state. The stored energy is released to the translational modes by collisional deexcitation of this state; the principal molecules in the deactivation collisions are oxygen and water vapor. The deactivation time is so short compared to all hydrodynamic processes in the propagation problem that it may be regarded as zero. Hence, the energy deposition rate may be written as

$$\rho_0 \dot{Q}(r,t) = \alpha_{H_2O} I(r,t) + \rho_0 \dot{Q}'(r,t) \tag{30}$$

where $\rho_0 \dot{Q}'$ is the energy deposition rate due to all other constituents of air.

Figure 1 is an energy level diagram showing the principal lower vibrational levels of CO_2, N_2, and H_2O. The excited levels of the various molecules are populated according to Boltzmann statistics; therefore CO_2 molecules in the (100) state are always present and beam photons may be absorbed, leaving the CO_2 molecules in the (001) state.
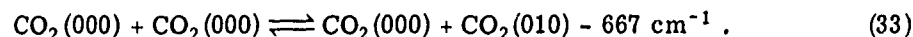
The reaction

$$CO_2(001) + N_2 \rightleftharpoons CO_2(000) + N_2^* + 18 \text{ cm}^{-1} \tag{31}$$
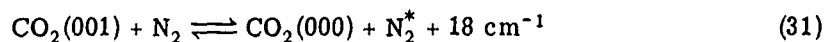
is very rapid due to resonance between the levels of CO_2 and N_2^*, the characteristic time being of the order of 10^{-7} sec. The system of carbon dioxide molecules is thus displaced from a thermal equilibrium distribution with an excess of molecules in the ground state and the (001) state, and a deficiency in the (100) level. The latter state will be repopulated principally by collisions of the type

$$CO_2(010) + CO_2(010) \rightleftharpoons CO_2(100) + CO_2(000) - 54 \text{ cm}^{-1} . \tag{32}$$
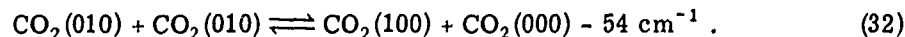
This reaction proceeds faster than all others that tend toward the same final state because of resonance. The energy removed in this reaction comes from the translational modes. Reaction (32) tends to deplete the supply of (010) levels, but these are replenished through the process

$$CO_2(000) + CO_2(000) \rightleftharpoons CO_2(000) + CO_2(010) - 667 \text{ cm}^{-1} . \tag{33}$$

The absorbed energy in Reaction (33) once again comes from translation. Two reactions of type (33) must occur for every one of the type indicated by Reaction (32) to maintain the CO_2 in thermal equilibrium. The removal of energy from the translational modes by Reactions (32) and (33) cools the CO_2 molecular system, and, concomitantly, the air. Because the reactions subsequent to the photon absorption that are described above occur so rapidly as to be almost instantaneous, the rate of energy removal from the translational modes is governed by the rate at which photon absorption occurs. Therefore the contribution of the CO_2 molecules to $\rho_0 \dot{Q}'$ is given by
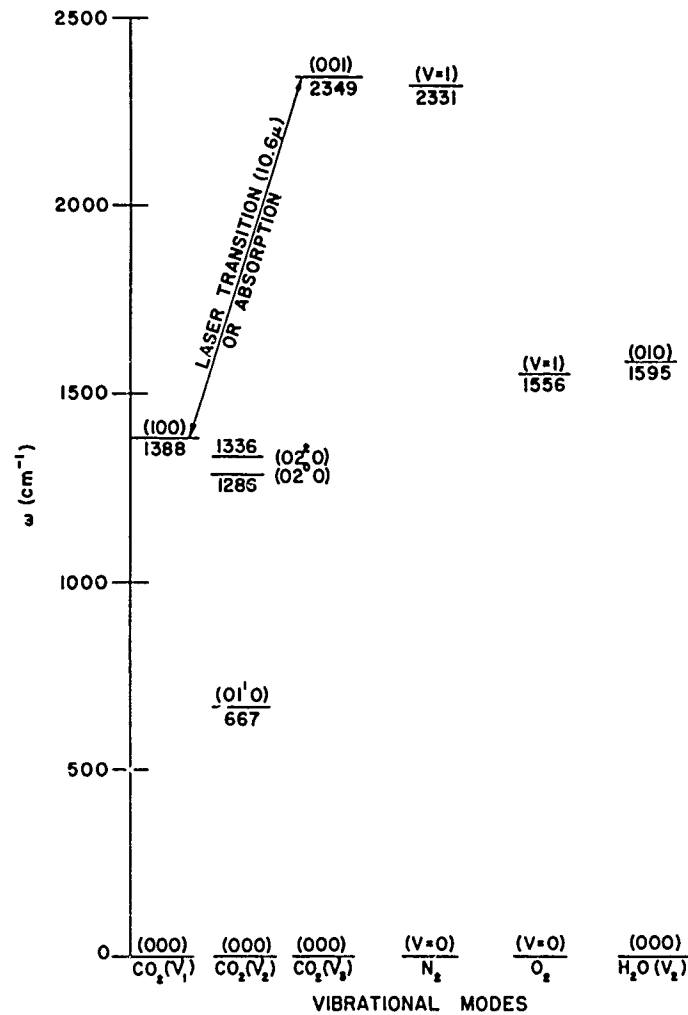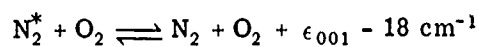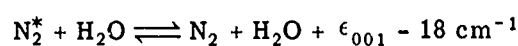
Fig. 1 - The principal lower vibrational energy levels of the major constituents of air—CO_2, N_2, O_2, and H_2O—are shown, with the 10.6-micron laser transition explicitly marked. The 10.6-micron photon energy is designated as $\hbar\omega_\gamma$.

$$\rho_0 \dot{Q}'_{CO_2} = -\frac{\epsilon_{100}}{\hbar\omega_\gamma} \alpha_{CO_2} I(r,t) \ . \tag{34}$$

Reaction (31) is populating the N_2^* above the equilibrium level; simultaneous with the CO_2 collisions, N_2^* is undergoing collisions of the form

$$N_2^* + O_2 \rightleftharpoons N_2 + O_2 + \epsilon_{001} - 18 \text{ cm}^{-1}$$

and   (35)

$$N_2^* + H_2O \rightleftharpoons N_2 + H_2O + \epsilon_{001} - 18 \text{ cm}^{-1}$$

which tend to depopulate the excited level N_2^*. In addition to Reactions (35), depopulation may go via excited states of O_2 and H_2O, and Reactions (35) will be understood to symbolize both. When water vapor is present in any significant amount, deactivation of nitrogen proceeds primarily along the second route; since the water vapor content of air is a variable quantity, both reactions must be included.

Let δN_2^* represent the excess number of N_2^* molecules at time t over the equilibrium number at some point r in the beam. Its time rate of change is given by

$$\frac{d}{dt} \delta N_2^* = \frac{\alpha_{CO_2}}{\hbar\omega_\gamma} I(r,t)$$

$$- \delta N_2^* \left\{ \beta_{N_2^*O_2 \rightarrow N_2O_2} N_{O_2} + \beta_{N_2^*H_2O \rightarrow N_2H_2O} N_{H_2O} \right\} \qquad (36)$$

where the quantity β is the reaction constant for the reactions indicated by the subscripts (12), and N_{O_2} is the number density of O_2 molecules, and N_{H_2O} the number density of water molecules. In terms of a reaction time τ, the above equation may be rewritten as

$$\frac{d}{dt} \delta N_2^* = \frac{\alpha_{CO_2}}{\hbar\omega_\gamma} I(r,t) - \frac{\delta N_2^*}{\tau} \qquad (37)$$

where

$$\frac{1}{\tau} = \frac{1}{\tau_{N_2^*O_2}} \frac{p(O_2)}{P} + \frac{1}{\tau_{N_2^*H_2O}} \frac{p(H_2O)}{P} \quad , \qquad (38)$$

$p(O_2)$ and $p(H_2O)$ are the partial pressures of O_2 and H_2O, respectively, P is the total pressure, and $\tau_{N_2^*O_2}$ and $\tau_{N_2^*H_2O}$ are the reaction times for Reactions (35). The derivative is the substantial time derivative and, for the steady-state case, the solution to the above equation becomes

$$\delta N_2^*(r) = \frac{\alpha_{CO_2}}{v_0 \hbar\omega_\gamma} \int_{-\infty}^{0} ds \, I(r + s\hat{v}_0) \, e^{\frac{s}{v_0\tau}} \quad . \qquad (39)$$

The number of energy-releasing transitions per second is $\delta N_2^*/\tau$ and the rate of energy release is

$$\frac{\epsilon_{001}}{\hbar\omega_\gamma} \frac{\alpha_{CO_2}}{v_0\tau} \int_{-\infty}^{0} ds \, I(r + s\hat{v}_0) \, e^{\frac{s}{v_0\tau}} \quad . \qquad (40)$$

The total energy deposition rate is obtained by combining Eqs. (30), (34), and (40)

$$\rho_0 \dot{Q} = \left(\alpha_{H_2O} - \frac{\epsilon_{100}}{\hbar\omega_\gamma} \alpha_{CO_2} \right) I(r)$$

$$+ \frac{\epsilon_{001}}{\hbar\omega_\gamma} \frac{\alpha_{CO_2}}{v_0\tau} \int_{-\infty}^{0} ds \, I(r + s\hat{v}_0) \, e^{\frac{s}{v_0\tau}} \quad . \qquad (41)$$

This last result, taken together with the steady-state solutions of the linearized hydro-dynamic equations, yields, after evaluation of some integrals,

$$\rho_1(r) = \frac{p_1(r)}{c_s^2}$$

$$- \frac{(\gamma - 1)}{v_0 c_s^2} \; \alpha \int_{-\infty}^{0} ds \left(1 - \delta \, e^{\frac{s}{v_0 \tau}}\right) I(r + s\hat{v}_0) \tag{42}$$

where

$$\alpha = \alpha_{CO_2} + \alpha_{H_2O} \tag{43}$$

and

$$\delta = \frac{\epsilon_{001}}{\hbar\omega_\gamma} \; \frac{\alpha_{CO_2}}{\alpha} \; . \tag{44}$$

In addition, the fact that

$$\epsilon_{001} - \epsilon_{100} = \hbar\omega_\gamma \tag{45}$$

has been incorporated into Eq. (42).

The quantities α_{CO_2} and α_{H_2O} for air are related (13, 14) to the partial pressures of CO_2 and water vapor, temperature, and total pressure by

$$\alpha_{CO_2} = 1.44 \times 10^{-3} \left(\frac{295}{T}\right)^{1\,5} 10^{-\frac{970}{T}} \; \text{cm}^{-1} \tag{46}$$

and

$$\alpha_{H_2O} = 4.32 \times 10^{-11} p(H_2O)[P + 193p(H_2O)] \; \text{cm}^{-1} \; . \tag{47}$$

The absorption coefficient of water vapor in air used here has been determined empirically only in the temperature range of 23°C to 26°C; therefore, Eq. (47) has a limited temperature range of validity that must be borne in mind.

If the deactivation time τ of nitrogen were zero, then there would be no delay between the time of photon absorption and the appearance of the photon energy as heat. This is manifest in Eq. (42) where the term in the integrand that involves τ would not be present, and the density change ρ_1 would always be negative, i.e., the air always expands in the presence of the beam. Since τ in general does not vanish, varying amounts of heating and/or cooling may take place. For the case of no water vapor in the air at all, $\alpha_{H_2O} = 0$ and $\delta = 2.441$, while τ assumes its maximum value. Thus, for large velocities, i.e., for v_0 such that $v_0 \gg a/\tau$ throughout the beam, the factor $(1 - \delta)$ in the integrand multiplying the intensity becomes -1.44, so that $\rho_1 > 0$ and the beam absorption causes cooling. For lesser wind speeds and increasing water vapor content, the physical situation will be intermediate to these two extremes, but it should be noted that there can be no net cooling when $\alpha_{H_2O} > 1.44 \, \alpha_{CO_2}$.

The density change, as expressed in Eq. (47) (with the pressure term neglected), is related to the wave function φ by Eq. (4):

$$\rho_1(r) = -\frac{(\gamma-1)\alpha}{v_0 c_s^2}\, e^{-\alpha z} \int_{-\infty}^{0} ds\, \left(1 - \delta\, e^{\frac{s}{v_0 \tau}}\right) \frac{c}{8\pi}\, |\varphi(r + s\hat{v}_0)|^2 \ . \tag{48}$$

The dielectric constant $\epsilon^{(r)}$ is related to the index of refraction by

$$\epsilon^{(r)} = n^2 \ . \tag{49}$$

and the index of refraction is a function of density through the Lorentz-Lorenz law

$$\frac{n^2 - 1}{n^2 + 2} = N\rho \ . \tag{50}$$

In Eq. (50), ρ is the absolute density and N is the molecular refractivity. Since ρ_0 and ρ_1 are both small quantities, Eq. (50) may be rewritten, ignoring quadratic terms in ρ_1, as

$$n^2 - n_0^2 = 3N\rho_1 \ . \tag{51}$$

With Relations (51) and (48) included, Eq. (1) becomes

$$2ik\, \frac{\partial \varphi}{\partial z} + \nabla_\perp^2 \varphi$$

$$- \frac{3N(\gamma-1)\alpha k^2}{v_0 c_s^2}\, e^{-\alpha z}\varphi \int_{-\infty}^{0} ds\, \left(1 - \delta e^{\frac{s}{v_0 \tau}}\right) \frac{c}{8\pi}\, |\varphi(r + s\hat{v}_0)|^2 = 0 \tag{52}$$

which is the fundamental equation to be solved for the description of the propagation of a laser beam in the presence of a steady wind. The boundary conditions involve only the specification of the function φ on the plane $z = 0$. Equation (52) is clearly nonlinear and is not tractable from an analytic standpoint. Therefore it is solved by numerical computation.

III. COMPUTATIONAL METHODS

Transformation to Scaled Variables

Equation (52) is scaled for purposes of numerical computations. Let a be a length characterizing the initial beam profile in a direction transverse to the beam axis. New coordinates $\bar{x}$, $\bar{y}$, and ζ are defined by

$$\bar{x} = x/a$$

$$\bar{y} = y/a \tag{53}$$

$$\zeta = z/ka^2 \ .$$

A dimensionless wave function f is introduced by putting

$$f(\bar{x}, \bar{y}, \zeta) = \sqrt{\frac{ca^2}{8\pi P}}\, \varphi(x, y, z) \tag{54}$$

where P is the total luminous power output of the laser. The constant of the motion, given by Eq. (2), can be stated in terms of f by the requirement that

$$\iint\limits_{\zeta = \text{constant}} |f(\bar{x}, \bar{y}, \zeta)|^2 \, d\bar{x}\, d\bar{y} = 1 \ . \tag{55}$$

Combining Eqs. (53) and (54) with Eq. (52), the equation for the scaled amplitude f is

$$2i\, \frac{\partial f}{\partial \zeta} + \bar{\nabla}_{\perp}^2 f - \beta e^{-(ka^2\alpha)\zeta} f \int_{-\infty}^{0} ds \left(1 - \delta e^{\frac{as}{v_0 \tau}}\right) |f|^2 = 0 \tag{56}$$

where

$$\beta = \frac{3N(\gamma - 1)\, k^2}{c_s^2} \frac{\alpha P a}{v_0} \ . \tag{57}$$

(When a slewing beam is being studied, v_0 in Eqs. (56) and (57) is to be replaced by $v_0 + \Omega z$.)

Because Eq. (56) is parabolic, specification of the amplitude at the plane $\zeta = 0$ determines the function everywhere else; in particular, the values of f at any point in a given plane $\zeta = $ constant can be determined. The technique to be used for a numerical computation of solutions of Eq. (56) will be the replacement of Eq. (56) by an appropriate difference equation which will be used to solve for the solution at successive planes separated by distances limited only by considerations of accuracy and stability. The method of proceeding from plane to plane is referred to as "marching." (Because of the character of the boundary conditions of the problem and of the difficulties encountered in the numerical solution of hyperbolic equations by difference techniques, the approximation of neglecting the second derivative of φ with respect to z, used to derive Eq. (1), is essential to a numerical solution of the problem. Marching does not work for hyperbolic equations.)

Since a partial differential equation does not uniquely determine a corresponding difference equation, there are many candidates for the difference equation to be used in the numerical computation. Each candidate must meet the requirements of convergence (to insure that the solution of the difference equation converges to the solution of the differential equation for any ζ in the limit that $\Delta\bar{x}$ and $\Delta\bar{y}$ vanish) and of stability (which assures, to a limited degree, that the numerical solution of the difference equation remains reasonably close to the exact solution of the difference equation.)

Harmuth (15) has shown that a simple forward differencing of the linearized version of Eq. (56) (obtained by replacing the integral by its upper bound) is unstable for all choices of step size $\Delta\zeta$ and mesh sizes $\Delta\bar{x}$, $\Delta\bar{y}$. A symmetric differencing, or "two-point predictor," is stable, however, for a nonempty domain of the parameters $\Delta\zeta$, $\Delta\bar{x}$, $\Delta\bar{y}$. For integration in ζ, therefore, the derivative in ζ is replaced by

$$\left.\frac{\partial f}{\partial \zeta}\right|_{\bar{x},\bar{y},\zeta} = \frac{f(\bar{x},\bar{y},\zeta + \Delta\zeta) - f(\bar{x},\bar{y},\zeta - \Delta\zeta)}{2\Delta\zeta} \tag{58}$$

while the algorithm for the linearized version of Eq. (56),

$$2i\,\frac{\partial f}{\partial \zeta} + \frac{\partial^2 f}{\partial \bar{x}^2} + \frac{\partial^2 f}{\partial \bar{y}^2} + \beta M f = 0 \,, \tag{59}$$

is taken to be

$$2i\left[\frac{f(\bar{x},\bar{y},\zeta + \Delta\zeta) - f(\bar{x},\bar{y},\zeta - \Delta\zeta)}{2\Delta\zeta}\right] =$$

$$-\left[\frac{f(\bar{x} + \Delta\bar{x},\bar{y},\zeta) - 2f(\bar{x},\bar{y},\zeta) + f(\bar{x} - \Delta\bar{x},\bar{y},\zeta)}{(\Delta\bar{x})^2}\right]$$

$$-\left[\frac{f(\bar{x},\bar{y} + \Delta\bar{y},\zeta) - 2f(\bar{x},\bar{y},\zeta) + f(\bar{x},\bar{y} - \Delta\bar{y},\zeta)}{(\Delta\bar{y})^2}\right]$$

$$- \beta M f(\bar{x},\bar{y},\zeta) \,. \tag{60}$$

In Eq. (59), M is taken to be the maximum value of the integral in Eq. (56).

The stability and convergence properties of the linear algorithm given in Eq. (60), which are necessary (but not sufficient) conditions to the stability and convergence of the nonlinear algorithm, may be studied (16) by examining the Fourier components of all solutions to Eqs. (59) and (60). If a plane wave solution to Eq. (59) is taken as

$$f = U(\zeta)\, e^{i p \bar{x}} e^{i q \bar{y}} \tag{61}$$

then

$$U(\zeta) = e^{-i(p^2 + q^2 - \beta M)\zeta/2} \tag{62}$$

Assuming a solution of the form given by Eq. (61) for the difference Eq. (60), the $U(\zeta)$ now has two solutions (as opposed to one for the differential equation):

$$U_{\pm}(\zeta) = \left(iB \pm \sqrt{1 - B^2}\right)^{\Delta\zeta/2} \tag{63}$$

where

$$B = 2\Delta\zeta \left(-\frac{\sin^2(p\Delta\bar{x}/2)}{(\Delta\bar{x})^2} - \frac{\sin^2(q\Delta\bar{y}/2)}{(\Delta\bar{y})^2} + \frac{\beta M}{4}\right).$$

It is necessary to show that there exists a linear combination $V(\zeta)$ of the two solutions given in Eq. (63) that converges to Eq. (62) in the limit where $\Delta\zeta$, $\Delta\bar{x}$, and $\Delta\bar{y}$ vanish in some specified order and, to insure stability, that $V(\zeta)$ has the property that it grows as

$$\lim_{\zeta \to \infty} V(\zeta) \sim 0\left(\frac{1}{\Delta\zeta}\right). \tag{64}$$

If $(\Delta\bar{x})^2$ and $(\Delta\bar{y})^2$ are required to vanish in proportion to $\Delta\zeta$, then it can be shown that

$$\lim_{\Delta\zeta\to0} U_+(\zeta) = e^{-i(p^2+q^2-\beta M)\zeta/2}$$

while the solution $U_-(\zeta)$ fails to converge. The convergence of the solution of the difference equation to that of the differential equation can be assured if there exists a means of suppressing all those Fourier components of the type $U_-(\zeta)$. The unwanted solution in the general case may be suppressed by a "careful" specification of the function f at the plane $\zeta = 0$ *and* at the plane $\zeta = \Delta\zeta$. By "careful," one means that the specification at $\zeta = \Delta\zeta$ must be at least as accurate (17) as a Taylor's expansion about $\zeta = 0$ to the same order as the predictor algorithm. In this case, the algorithm is accurate to order $(\Delta\zeta)^2$, as is demonstrated that

$$\frac{f(\zeta+\Delta\zeta) - f(\zeta-\Delta\zeta)}{2\Delta\zeta} = \frac{1}{2\Delta\zeta}\left[f(\zeta) + \Delta\zeta\frac{\partial f}{\partial\zeta} + \frac{1}{2}(\Delta\zeta)^2\frac{\partial^2 f}{\partial\zeta^2} + \theta(\Delta\zeta^3)\right]$$

$$-\frac{1}{2\Delta\zeta}\left[f(\zeta) - \Delta\zeta\frac{\partial f}{\partial\zeta} + \frac{1}{2}(\Delta\zeta)^2\frac{\partial^2 f}{\partial\zeta^2} + \theta'(\Delta\zeta^3)\right]$$

$$= \frac{\partial f}{\partial\zeta} + \theta''(\Delta\zeta^3) \ . \tag{65}$$

Thus at $\zeta = \Delta\zeta$, the data must be specified as

$$f(\Delta\zeta) = f(0) + \Delta\zeta\frac{\partial f}{\partial\zeta}(0) + \frac{(\Delta\zeta)^2}{2}\frac{\partial^2 f}{\partial\zeta^2}(0) \tag{66}$$

where

$$2i\frac{\partial f}{\partial\zeta}(0) = -\bar{\nabla}_\perp^2 f(\bar{x},\bar{y},0) - \beta f(\bar{x},\bar{y},0)\int_{-\infty}^0 ds\left(1 - \delta e^{\frac{\partial s}{v_0\tau}}\right)\Big|f\Big|^2_{\zeta=0} \tag{67}$$

and $\partial^2 f(0)/\partial\zeta^2$ must be similarly specified.

Since the unwanted solution has been suppressed by the above device, the test for linear stability need only be applied to the wanted solution, and, indeed, may be applied to its Fourier components which are primarily characterized by the function $U_+(\zeta)$. The stability requirement on $U_+(\zeta)$ given by Eq. (64) demands of B that

$$\Big|iB + \sqrt{1 - B^2}\Big| \le 1 \ . \tag{68}$$

Since B is a real number, if $B > 1$, Eq. (68) can never hold. A marginal stability is achieved only if $B < 1$. The conditions of stability, in terms of $\Delta\zeta$, $\Delta\bar{x}$, and $\Delta\bar{y}$, divide into three categories:

$$\beta M < 0 \ : \quad \left|\Delta\zeta\left(\frac{1}{\Delta\bar{x}^2} + \frac{1}{\Delta\bar{y}^2} + \frac{|\beta M|}{4}\right)\right| < \frac{1}{2}$$

$$0 < \frac{\beta M}{4} \le \frac{1}{2}\left(\frac{1}{\Delta\bar{x}^2} + \frac{1}{\Delta\bar{y}^2}\right) \ ; \quad \left|\Delta\zeta\left(\frac{1}{\Delta\bar{x}^2} + \frac{1}{\Delta\bar{y}^2} - \frac{|\beta M|}{4}\right)\right| < \frac{1}{2}$$

$$\frac{1}{2}\left(\frac{1}{\Delta\bar{x}^2} + \frac{1}{\Delta\bar{y}^2}\right) < \frac{\beta M}{4} \ ; \quad \frac{\Delta\zeta\beta M}{4} < \frac{1}{2} \ . \tag{69}$$

With a prescribed choice of $\Delta\bar{x}$ and $\Delta\bar{y}$ the numerical solution of the difference equation will be unstable unless $\Delta\zeta$ is chosen to satisfy the three conditions in Eq. (69). Since the first condition is the most stringent of all three restrictions, choosing $\Delta\zeta$ in accord with it will ensure the desired stability.

The intrusion of βM into the stability conditions given in Eq. (69) may be viewed in a different light. The solution of Eq. (59) may be written in the form

$$f = e^{-i\frac{\beta M \zeta}{2}} g$$

where g is a solution of the equation

$$2i \frac{\partial g}{\partial \zeta} + \bar{\nabla}_\perp^2 g = 0 .$$

In order that a numerical solution of the equation be satisfactory, the oscillations, in ζ, of the exponential factor must be sampled by at least six points per oscillation. Thus, step sizes $\Delta\zeta$ must be chosen so that

$$\Delta\zeta\beta M \leq 2\pi/3 \sim 2$$

which is the same as the last condition of Eq. (69).

All the above considerations apply, of course, only to the linear approximation. Notwithstanding the choice of M as the maximum of the integral, the predictor was found to be incapable of suppressing a nonlinear instability for values of β of interest even though the first criterion of Eq. (69) was well satisfied. In order to damp the nonlinear growth, a simple two-point corrector (18) was applied in conjunction with the predictor. Writing out the terms of order $\Delta\zeta^3$ explicitly, the predictor and corrector are taken as

$$f^{(p)}(\zeta + \Delta\zeta) = f(\zeta - \Delta\zeta) + 2\Delta\zeta \frac{\partial f(\zeta)}{\partial \zeta} - \frac{(\Delta\zeta)^3}{3} \frac{\partial^3 f(\zeta)}{\partial \zeta^3}$$

and

$$f^{(c)}(\zeta + \Delta\zeta) = f(\zeta) + \frac{1}{2} \Delta\zeta \left[\frac{\partial f^{(p)}(\zeta + \Delta\zeta)}{\partial \zeta} + \frac{\partial f(\zeta)}{\partial \zeta} \right] + \frac{(\Delta\zeta)^3}{12} \frac{\partial^3 f(\zeta)}{\partial \zeta^3} . \tag{70}$$

When $\Delta\zeta$ is taken small enough, the third derivatives in both of the expressions of Eq. (70) become equal in value; the correct value of f at the plane $\zeta + \Delta\zeta$ is then taken to be that linear combination of the corrector and predictor that eliminates the terms of order $\Delta\zeta^3$, that is,

$$f(\zeta + \Delta\zeta) = 0.2 f^{(p)}(\zeta + \Delta\zeta) + 0.8 f^{(c)}(\zeta + \Delta\zeta) . \tag{71}$$

In Eq. (70), the first derivatives are evaluated by the use of the algorithm that relates these derivatives to the transverse derivatives and the heating integral at the plane ζ, just as Eq. (67) does so at the plane which is the face of the laser. This form of the algorithm has been found to be sufficient to suppress the nonlinear growth and has been used in this work.

It is convenient (19) to make a change of variables in order to map the whole transverse plane into a finite region. The following transformations were chosen:

$$\bar{x} = \ln\left[\xi'(4-\xi)\right]$$

$$\bar{y} = \ln\left[\eta'(4-\eta)\right] \quad . \tag{72}$$

The transverse Laplacian, in terms of the new variables ξ and η, now becomes

$$\frac{\xi^2(4-\xi^2)}{16}\frac{\partial^2 f}{\partial\xi^2} + \frac{(4-2\xi)(4-\xi)}{16}\frac{\partial f}{\partial\xi}$$

$$+ \frac{\eta^2(4-\eta^2)}{16}\frac{\partial^2 f}{\partial\eta^2} + \frac{(4-2\eta)(4-\eta)}{16}\frac{\partial f}{\partial\eta} \quad . \tag{73}$$

In terms of these new variables, the conserved quantity (see Eq. (54)) takes the form

$$\int_0^4 d\xi \int_0^4 d\eta \frac{f_r^2 + f_i^2}{(4-\xi)\,\xi\,(4-\eta)\,\eta} = 1 \quad . \tag{74}$$

The left-hand side of Eq. (74) is monitored throughout every run as a check on the stability and convergence of the algorithm.

Laser beams whose transverse dimensions vary considerably with z present problems of sampling for numerical schemes with fixed transverse mesh size. In Appendix A, a formulation of the propagation problem is presented in terms of coordinates that will automatically take into account the change in the beam size. The stability and convergence criteria developed in this section may be applied to the equations of Appendix A with little modification.

IV. RESULTS OF NUMERICAL COMPUTATIONS

Accuracy Criteria

The computer code described in Section III has been run successfully for a large number of initial parameters. Because exact analytical solutions of the full nonlinear problems were lacking, criteria were needed for determining whether a given run led to correct results or not. Since comparisons with the exact solutions could be the only valid check on the numerical solutions, the computer code was applied to problems to which exact results were known. These solutions are discussed in Appendix B. Such checks provided a testing ground for certain parts of the numerical procedures used and served as a test bed for studying the effects of parameter such changes as step sizes, mesh sizes, focused coordinate systems, etc. These comparisons provided the necessary minimum level of confidence in the chosen algorithm needed to proceed with the nonlinear problems.

This section is devoted to a description of the criteria that were and are used to establish run quality, the characteristics of reliable and unreliable runs, and a delineation of the potential sources of error. These are illustrated by the presentation of some of the results obtained with the computer code.

Run Quality Criteria

Run quality is a function of the downrange distance z; a given run may be good up to one value of z, then poor thereafter. Clearly it is desirable to have runs of high quality for as large a value of range as possible.

It has been shown that the quantity

$$E = \iint_z |f|^2 \, dx \, dy$$

is a constant of the motion. The ratio

$$\delta E(z)/E = \frac{E(z) - E(0)}{E(0)}$$

provides a quantitative measure of numerical accuracy in numerical solutions. This quantity was determined, for the runs to be described later in this section, at selected intervals downrange, but in this report, its value will be given only at the last one or two values of z before run termination. Since $\delta E/E$ generally (but not always) increases with z, the final numbers are indicative of the accuracy upbeam.

A second qualitative measure of the validity of a calculation is the frequency with which the oscillations in the real and imaginary parts of the amplitude are sampled by the mesh. To each run, usually at the final one or two z values reported, a Run Quality Factor (RQF) is assigned according to the following conditions:

Sampling Characteristics	Run Quality Factor
Sampling nowhere exceeds 6 to 8 points of the mesh per oscillation.	POOR
Small amplitude oscillations sampled poorly; large amplitude oscillations sampled at least 6 to 8 times.	BORDERLINE
Large and small oscillations are sampled at least 6 to 8 times.	GOOD
Large and small oscillations are sampled better than 8 times.	EXCELLENT

Figures 2 and 3 show a plot of the real part of the amplitude at the mesh points taken from a typical set of runs demonstrating the sampling for different RQF's. Run quality factors are helpful in discussing run characteristics, but they must be used with caution since they can be misleading. An RQF of POOR may in fact be describing the oscillations quite faithfully; but usually poor runs, when continued downrange, lead rapidly to very large values of $\delta E/E$. A run with an RQF of EXCELLENT may be suffering from aliasing and, in fact, be quite poor; cases such as these may often be detected by looking at RQF as a function of z.

Further, RQF's are often difficult to assign; they are a function of mesh size as well, and they suffer to a degree from subjective interpretations. A cruder pair of
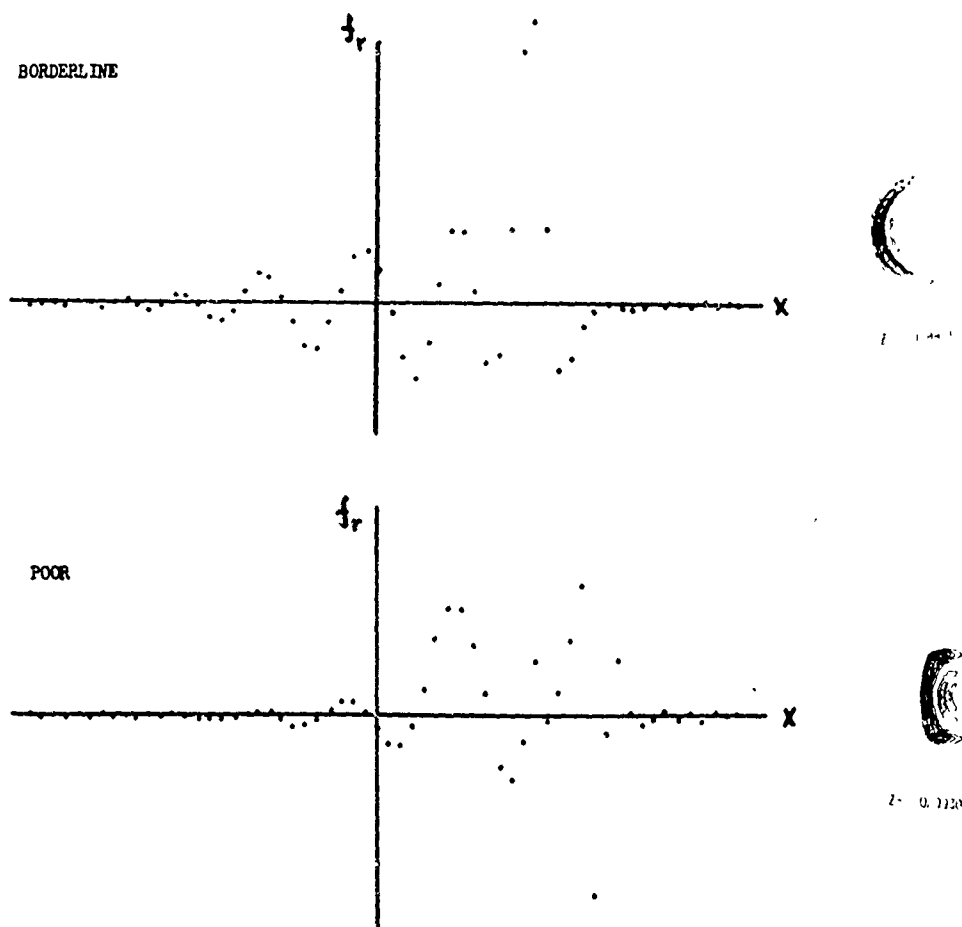
6106; P $= 2 \times 10^6$ watts; a = 25 cm; f = 1.0 km; L = 1.2 km;
Ω = .05 rad/sec; $p(H_2O)$ = 12 torr; v_0 = 1000 cm/sec.

Fig. 2 – Sampling quality of the real part of the amplitude along the line of symmetry graphically displayed for Run Quality Factors BORDERLINE and POOR.

categories such as acceptable runs and unacceptable runs may in some instances be satisfactory. Experience shows that POOR runs are *unacceptable*, while BORDERLINE, GOOD, and EXCELLENT runs are *acceptable*.

A third and very important criterion of run quality is provided by the appearance of isoirradiance contours in a beam cross section as a function of z. For a run of high quality, these contours evolve smoothly from concentric circles (for an initially rotationally symmetric beam) to crescent-shaped curves. Runs of poor reliability generally betray themselves by the development of straight lines about which the crescent patterns are forced to evolve. These lines, which are not isoirradiance contours, and hence are *not* plotted, run parallel to the mesh lines or at 45° to the mesh lines. There are two principle reasons for such development. First, in the case of a small f ratio, the initial amplitude will contain many oscillations in the aperture plane. A fine mesh is needed to sample these sufficiently frequently for a good description. Since a rectangular mesh is used, sampling along the 45° lines is less frequent than along the mesh lines themselves.

5257; $P = 10^6$ watts; $a = 25$ cm; $f = 2.0$ km; $L = 2.4$ km;
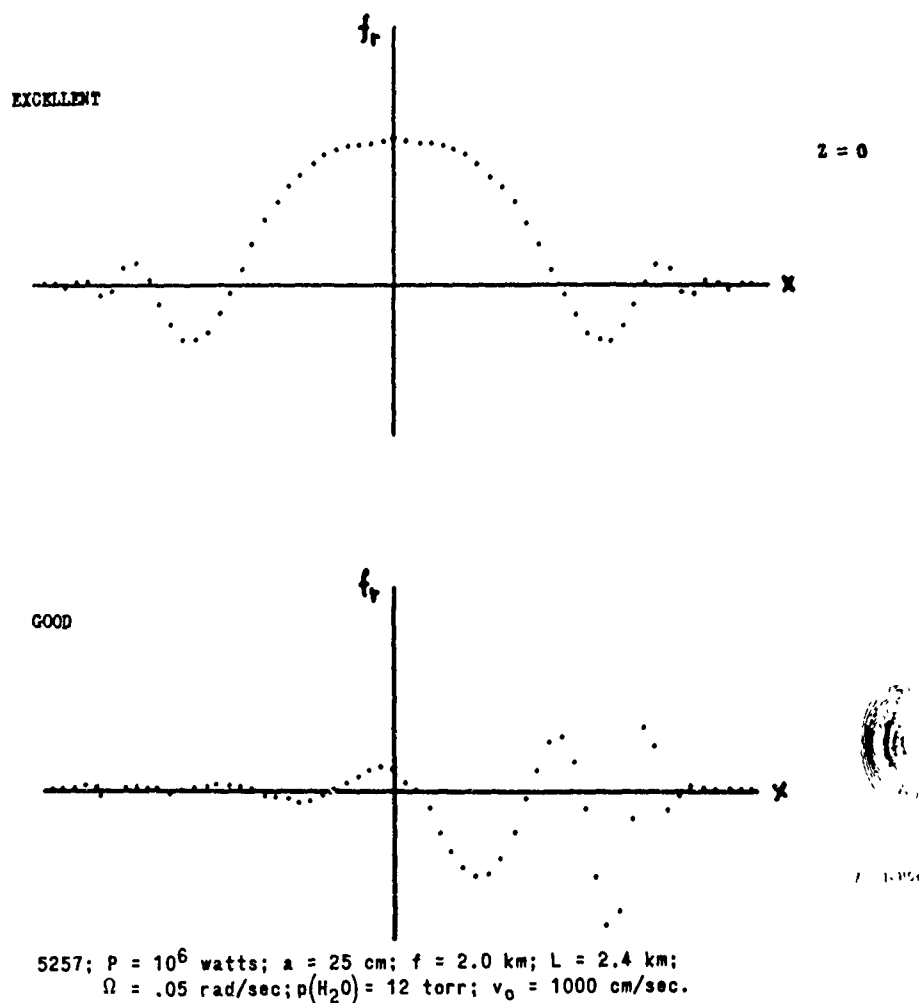$\Omega = .05$ rad/sec; $p(H_2O) = 12$ torr; $v_o = 1000$ cm/sec.

Fig. 3 – Sampling quality of the real part of the amplitude graphically
displayed for Run Quality Factors EXCELLENT and GOOD.

Mesh sizes that provide adequate sampling at the laser aperture may prove inadequate at
some distances downbeam, and errors are introduced into the numerical solution.

In the vacuum case, the errors possess a 90° rotational symmetry. When wind is
present, the symmetry in the errors deteriorates and is masked to some degree by the
aberrations due to heating. These effects are illustrated by the contour plots of Figs.
4 and 5. Figure 4 shows two vacuum runs for a Gaussian beam focused at 1 km; the
mesh number was 31 x 61 in both cases, but the sampling of the oscillations was altered
by using two different coordinate systems.* The contours in the top row were calculated
with $\ell = 1.5$ km, while those of the bottom row were calculated with $\ell = 1.12$ km. In the
first case, the beam is sampled well enough by the mesh at the laser aperture, but as the
beam converges toward the focus, the sampling becomes poorer. In the second case,
improvement is achieved for two reasons:

*See Appendix A for a discussion of focused coordinate systems and the significance of the param-
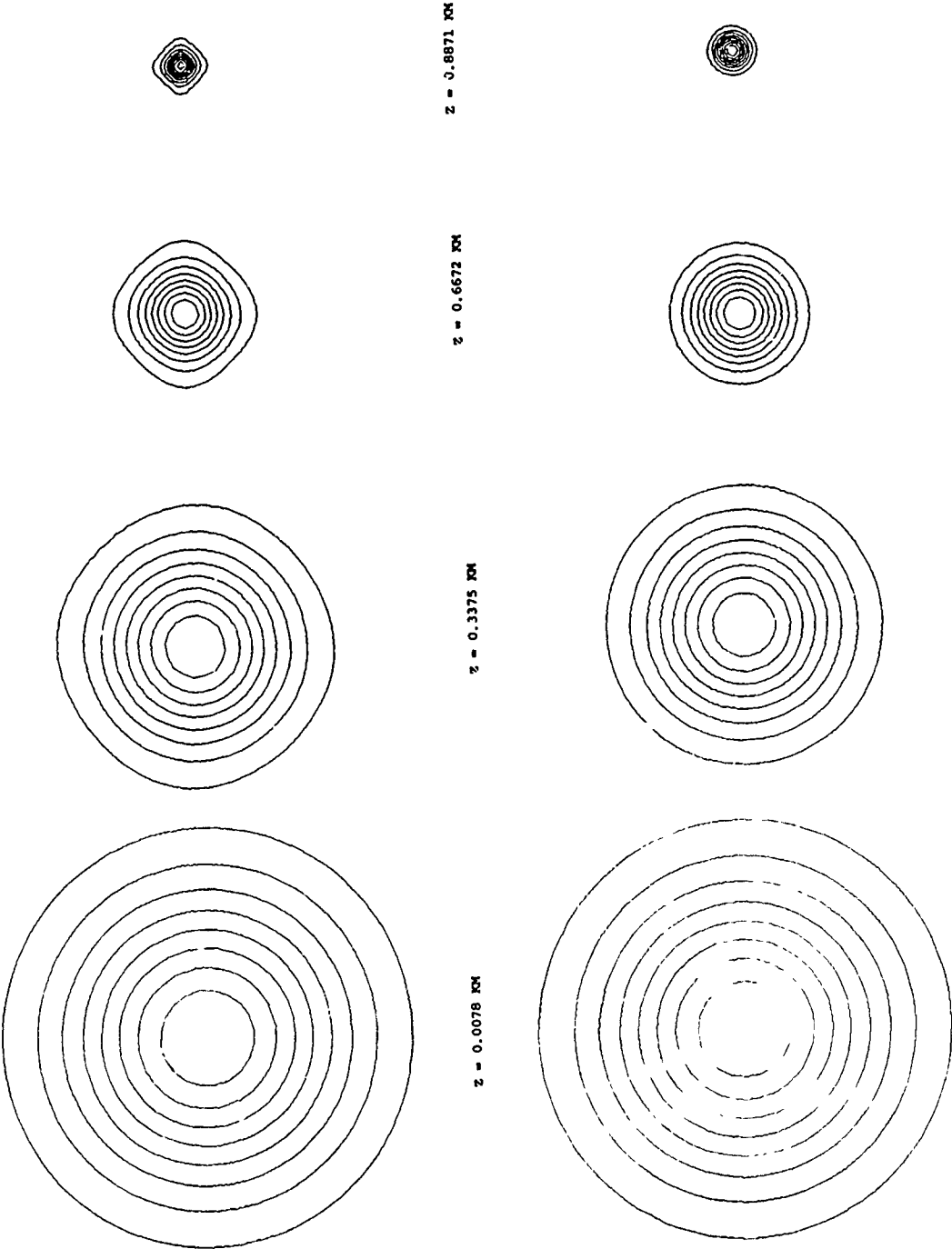eter ℓ mentioned in the above paragraph.

Fig. 4 — Vacuum runs for beams focused at 1 km: top row, ℓ = 1.50 km; bottom row, ℓ = 1.12 km; a = 25 cm.

1.   The beam is being specified on spherical surfaces, on which phase oscillations are small since the surfaces more closely approximate surfaces of constant phase than planes do.

2.   The mesh size shrinks in about the same proportion that the beam does, so that the beam is sampled with the same thoroughness downrange as it is at the aperture.

Figure 5 shows a run with atmospheric heating present, but with an inappropriate choice of focused coordinate system.   The outermost contours betray the poor sampling on the left (the wind moves from left to right), but the aberrations of the beam due to atmospheric heating mask this effect on the downwind side.   Secondly, contours may show an evolution about lines parallel to the mesh axes; such development arises, in part, for reasons of physics.   Any numerical scheme for solving Eq. (56) must rely on a mesh which samples only a part of space; a beam initially confined to that part of space covered by the mesh will ultimately grow in size unless self-trapping should occur.   This growth occurs both for vacuum beams and for beams traversing a medium.   Unless the mesh is chosen so as to be able to accommodate this increase in size, a point will be reached in the calculation where the beam amplitude in the outer regions of the mesh is large, and poor sampling or boundary conditions will begin to manifest themselves in the solution.   The isoirradiance contours become very complicated and show definite square edges, reflecting the presence of the edges of the mesh; for this reason, we describe such a situation by the phrase "the beam has hit the edges of the mesh."   Run quality at such downrange distances deteriorates completely, reflecting poor sampling, and instabilities arise leading to large values for $\delta E/E$.   Figure 7 shows the isoirradiance contours for such a case, which will be discussed below in greater detail.   In some instances, the options made available by the parameter ℓ in the focused coordinate systems enable the deterioration of the run to be postponed to larger values of z.   However, the conditions imposed upon the value of ℓ to improve sampling at the aperture for beams of small f ratio run counter to those arising from the need to avoid having the beam hit the edges of the mesh.   In cases where neither condition may be relaxed, the computer code cannot be relied upon to describe the correct physical situation.   Modifications of the code that will allow ℓ to vary with z in an appropriate manner appear to be a way of handling situations such as these, but such changes have not yet been incorporated into the program.

Numerical Results

Results of particular numerical solutions of the problem of laser beam propagation through a nonturbulent atmosphere are now presented.   The numbers attached to a given computation serve to designate it; the particular characteristics of the beam at the aperture are specified, followed by the run quality characteristics ($\delta E/E$ and RQF) at one or more distances downrange.   The figures show the isoirradiance contours at selected downrange distances.   (In these figures, the scale of each of the plots is set by the size of the first of the plots; the contours represent 90% of peak intensity, 80% of peak intensity, etc., from the inside out.   The actual value of the peak intensity and the deflection of the peak intensity point from the beam axis are data available from the computations in general, but in some of these early results shown here, they were not.)   A paragraph is devoted to a discussion of the results in each case.   It is emphasized here, and in the examination of individual runs, that *not all of the solutions presented here are to be regarded as acceptable*.   Indeed, unacceptable numerical results are presented to illustrate the characteristics of erroneous solutions that may arise from an uncritical use of the numerical procedures described in this report.
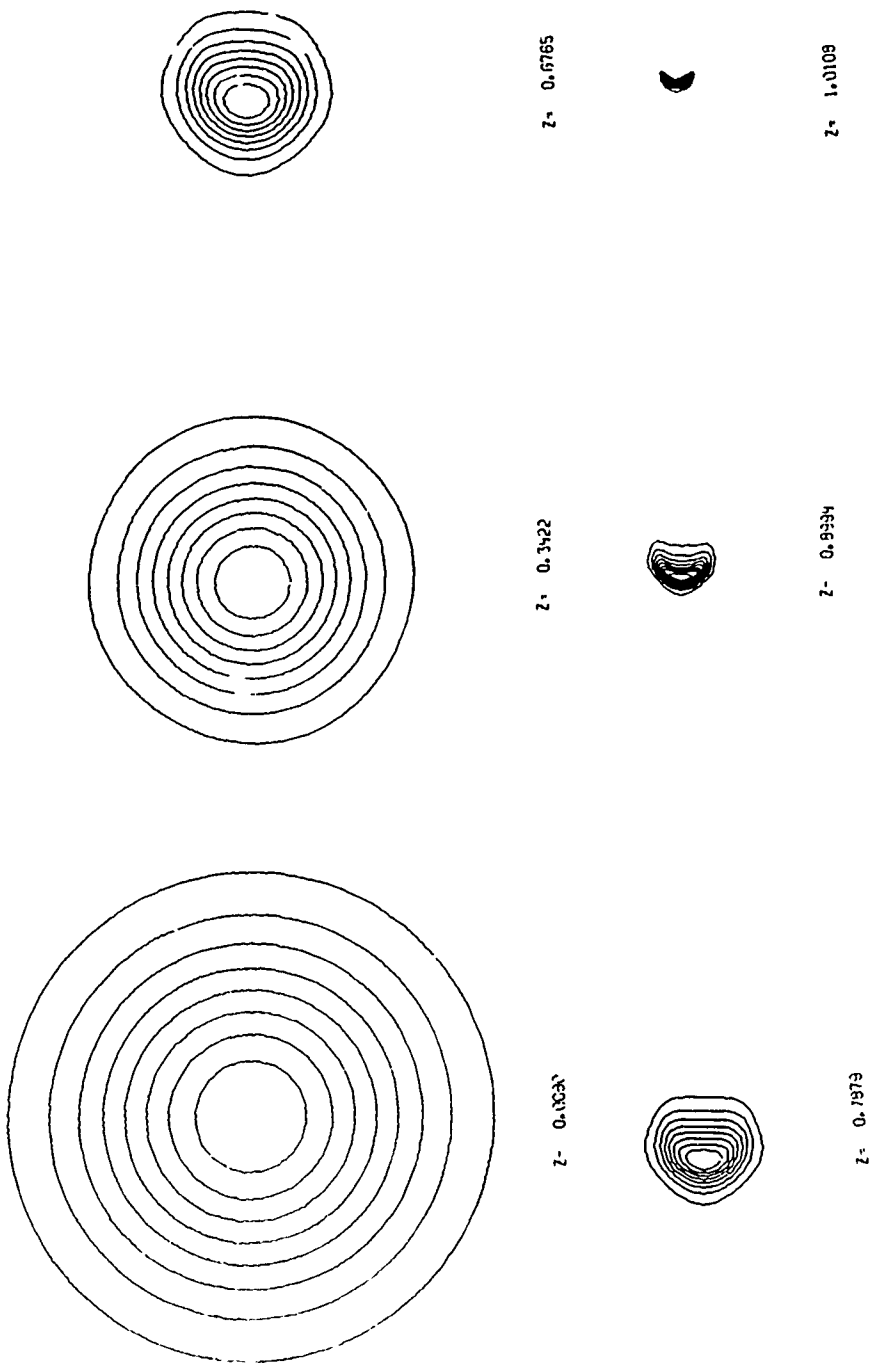
Fig. 5 — A run with atmospheric heating present but with a poor choice of focused coordinates, showing the associated beam squaring.
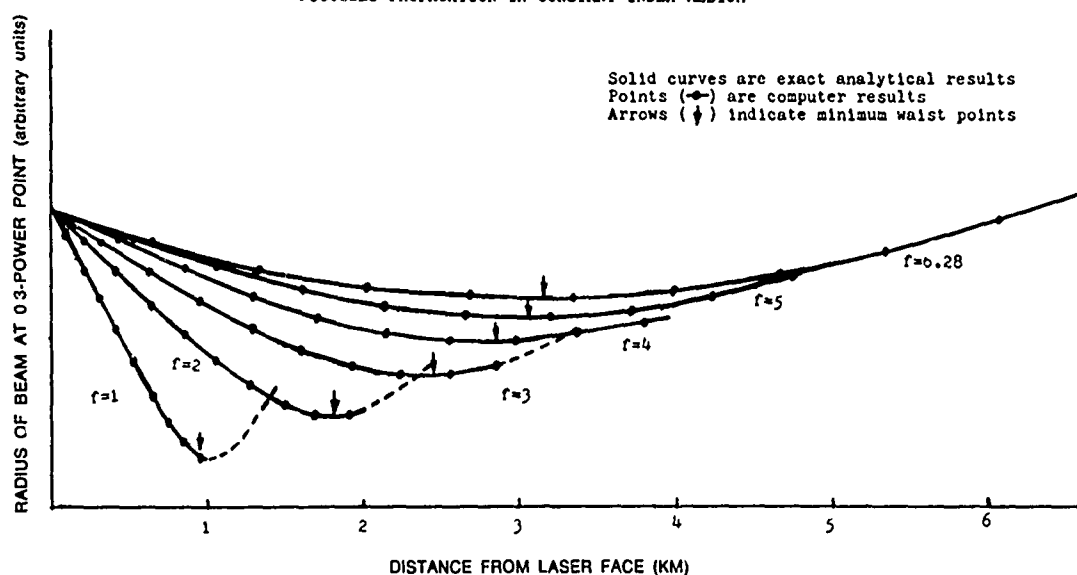
FOCUSSED PROPAGATION IN CONSTANT INDEX MEDIUM

Fig. 6 – Comparison of computer results with analytical results obtained from the theory of propagation of a focused laser beam in vacuum; a = 10 cm.

The graphs in Fig. 6 show light rays emanating from a point at the laser aperture where the power is 30% of the central intensity. The runs here are in vacuum to check the linear aspects of the code. The solid curves are analytical results, the points represent the computer results, and the arrows point to the waist of the beam. The agreement between theory and numerical computation is excellent. The runs in Fig. 6 were made with $\ell = 1.5f$ in all cases. Because the beam diverges to the right of the waist points, while the focused coordinate system continued to converge, the beams ultimately hit the edges of the mesh. The quantities $\delta E/E$, at the focal distances for the cases shown, were 6×10^{-4}, 7×10^{-4}, 8×10^{-4}, and 2×10^{-3} for the cases $f = 1, 2, 3,$ and 4 km, respectively, while for $f = 5$ and $f = 6$ km, $\delta E/E$ was 2×10^{-3} just short of the focal point in each case.

No-Diffraction Runs

No figure is provided here. The rationale for these runs is provided in Appendix B. These runs are made to check the nonlinear aspects of the code. This is done by dropping the Laplacian term in the wave equation, which is equivalent to saying that refraction dominates the character of the beam propagation. Such runs might be termed high-power runs, or no-diffraction runs, or the geometrical optics limit. The resultant equation, while still nonlinear, may be solved exactly (see Appendix B) to give the result that the intensity profile does not change downbeam. This result was confirmed by computation with the code by circumventing the subroutines that compute the Laplacian.
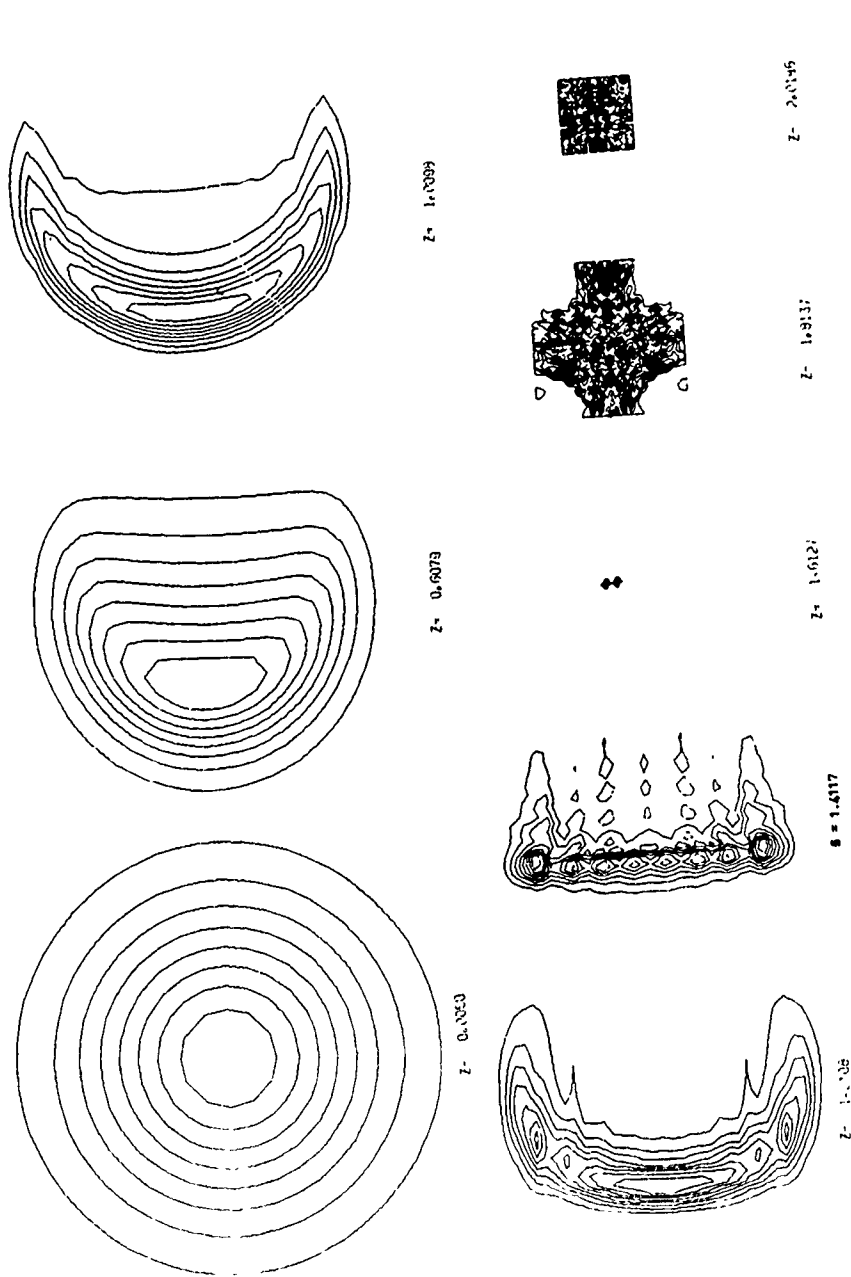
RUN #3346 (UNACCEPTABLE):   P = 10^5 watts; v_0 = 200 cm/sec;   a = 10 cm;   (21,41);

Ω = 0.0 rad/sec; δ = 0 (pure heating); f = 2 km; ℓ = 2.2km; α = .67 X 10^{-7} cm^{-1}.

Fig. 7 – Run No. 3346.

Run No. 3346, shown in Fig. 7, has the same parameters as those of the next two runs, illustrated in Figs. 8 and 9. This sequence of runs, together with the vac .um run for 2 km, shown in Fig. 6, illustrates the potential sources of error that may be encountered in these numerical computations as discussed earlier in this section. With no prior knowledge of the extent to which the beam would bloom, or diverge, because of the heating, a first guess was made that the choice of focused coordinates used for the vacuum case would work here. The first indication that this assumption was erroneous was provided by the isoirradiance contours at $z = 1.0098$ km; the maximum linear distance of the 0.3 isophote from the horizontal center line is the same as it was at the laser aperture while, for a vacuum run as seen from Fig. 6, it is only one-half as large. Thus, the heating effect is preventing the focusing of the beam, as it would otherwise do in vacuum. The coordinate system, on the other hand, is still converging so the beam will approach the edges of the mesh. At $z = 1.2108$ km, discernible flattening of the contours at right angles to the wind direction is perceived and become more pronounced at $z = 1.4117$ km. The structure at this point cannot be believed, even though $\delta E/E = 7 \times 10^{-4}$. (For this run, the RQF was not available. A reasonable guess can be made from the rapid variations of intensity across the beam that RQF here is POOR.) Succeeding isophote plots demonstrate the total deterioration of the run. At $z = 1.6127$ km, $\delta E/E \sim 10^{208}$, while at $z = 1.8337$ km, $\delta E/E = 5.91$.

It is important to note that the patterns at $z = 1.6127$ km, which so clearly show the unacceptable run quality, could easily have been missed had the computer been commanded to plot at slightly different z values. If fewer isoirradiance contours had been used, the plots at $z = 1.2608$ km and 1.4117 km would have shown less complexity and could then have been readily interpreted as complicated diffraction patterns. However, such interpretations were avoided by use of the $\delta E/E$ and RQF's.

The initial data shown in Fig. 8 are the same as the previous run; however, $\ell = \infty$, i.e., ordinary Cartesian coordinates were used, while $(N_x, N_y) = (31,61)$.

Because the previous run was so clearly in error, it became necessary to do the computation again. Since the beam did not appear to be focusing, Cartesian coordinates were used. At $z = 2$ km, $\delta E/E = 7 \times 10^{-5}$, but no RQF's were available in this early run. However the contours at $z = 2.0$ km show considerable flattening on the wind side of the beam. Beam deflection into the wind was enough to cause concern about poor sampling, so it was therefore decided that the run was UNACCEPTABLE.

Run No. 3353 of Fig. 9 is a repeat of the above two runs, but with $\ell = -2$ km. This choice of ℓ was taken because the coordinate system would then be slightly diverging, giving the beam more space in which to diverge. The differences between the isoirradiance contours at $z = 2$ km in this case and in the previous run are quite pronounced. The squaring of the pattern as seen in Fig. 8 is gone, and the contours on the wind side are less compressed. The value $\delta E/E = 2 \times 10^{-5}$ here, and the RQF was GOOD. It appears that the run could be further improved by choosing ℓ slightly closer to zero; however, this would sacrifice accuracy at the center of the beam for the same total number of mesh points. With the NRL computer, increasing the number of mesh points is not possible.

The contours show that the beam reaches a minimum size at approximately 1.2 km and diverges for larger values of z. Since the computer printout also included phase angle at each mesh point, the assessment that the beam is no longer focusing beyond 1.2 km could be verified by the behavior of the phase angle as a function of radial distance from the beam center. Phase angle should increase with radial distance for a diverging beam, and this was indeed the case here.
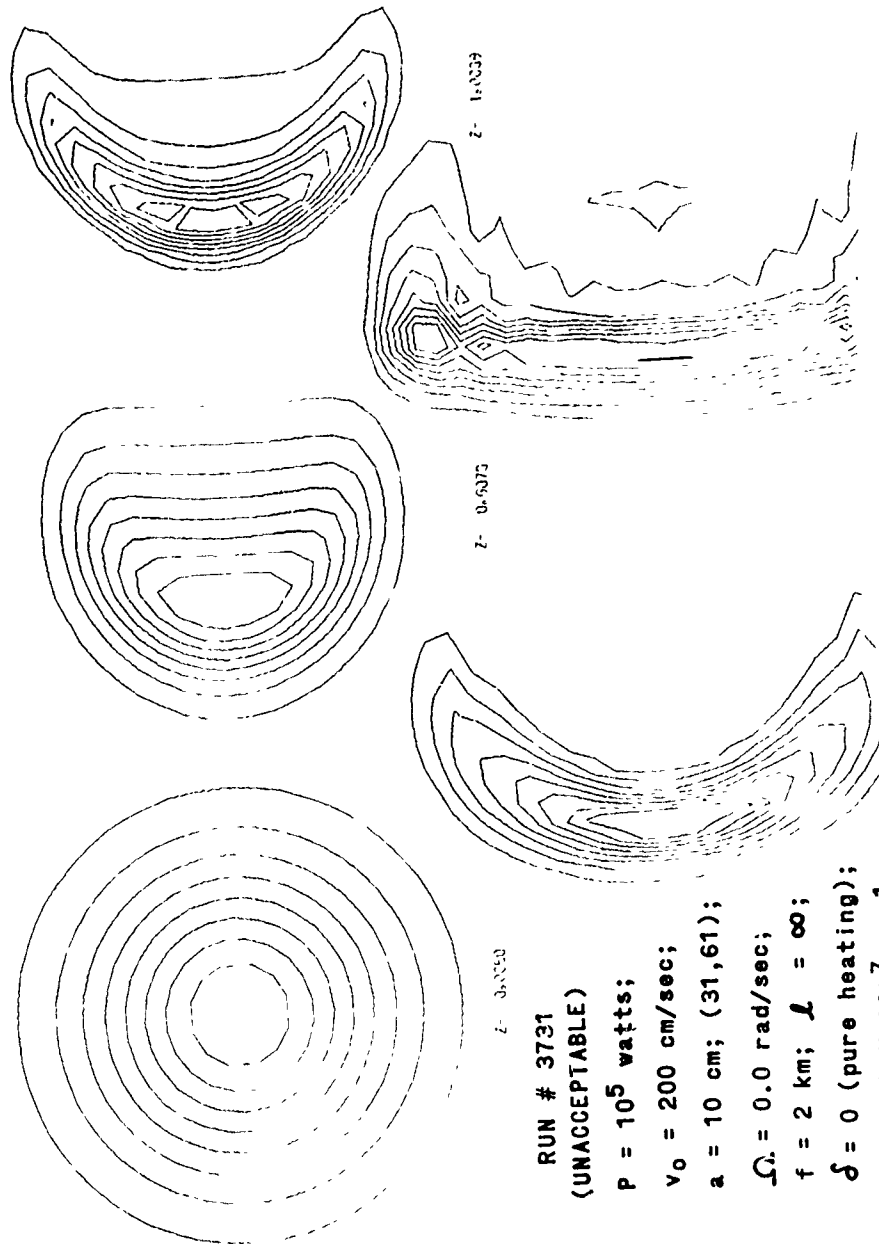
RUN # 3731
(UNACCEPTABLE)

$P = 10^5$ watts;

$v_0 = 200$ cm/sec;

$a = 10$ cm; (31,61);

$\Omega = 0.0$ rad/sec;

$f = 2$ km; $\mathcal{L} = \infty$;

$\delta = 0$ (pure heating);

$\alpha = .67 \times 10^{-7}$ cm^{-1}.

Fig. 8 – Run No. 3371.

RUN # 3353 (ACCEPTABLE)

$P = 10^5$ watts;

$v_0 = 10$ cm/sec;

$a = 10$ cm; (31,61);

$\Omega = 0.0$ rad/sec;

$f = 2$ km; $\ell = -2$ km;

$\delta = 0$ (pure heating);

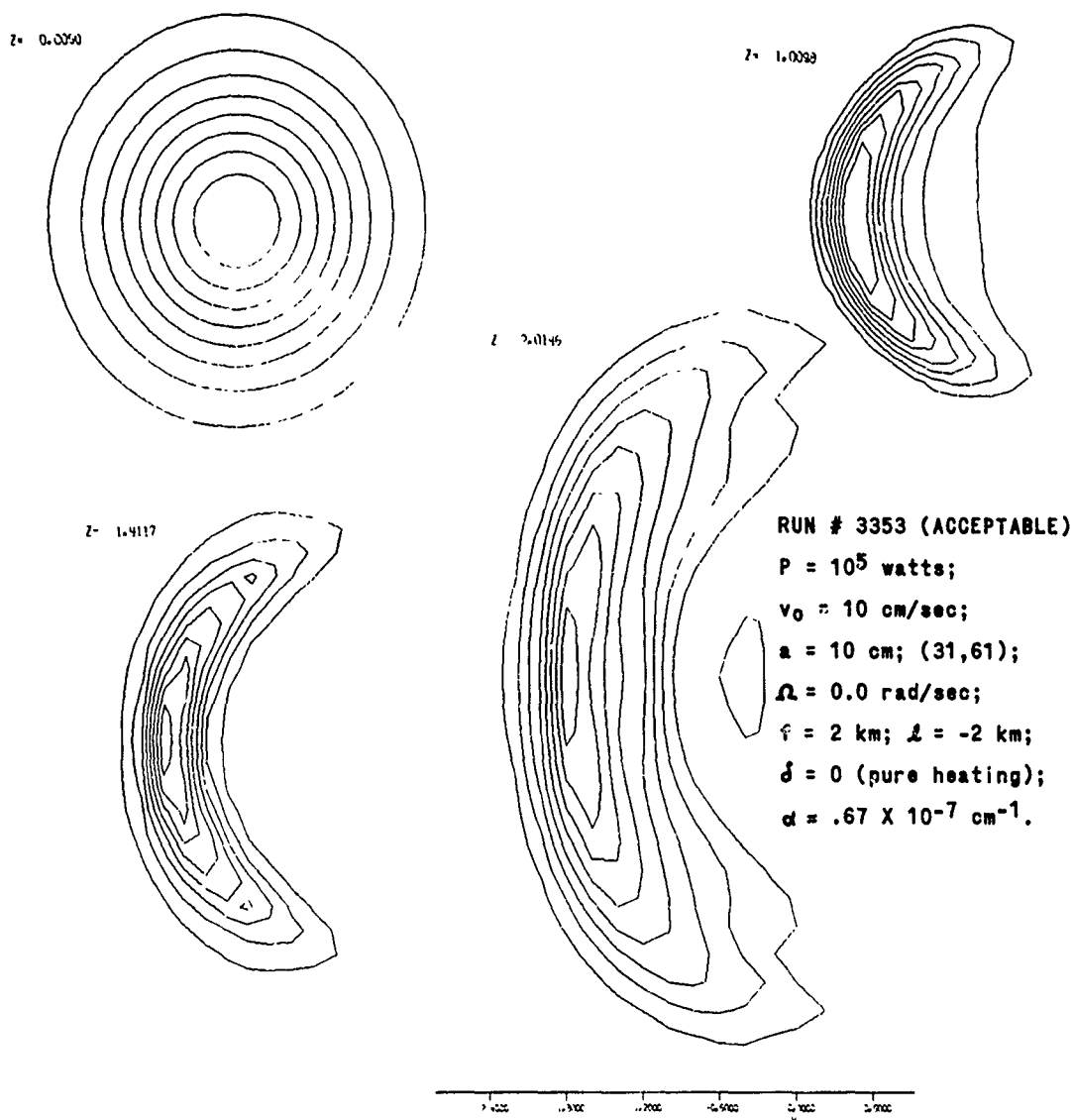$\alpha = .67 \times 10^{-7}$ cm^{-1}.

Fig. 9 – Run No. 3353.

The deflection of the peak intensity along the line of symmetry of the contour plot is plotted against range z in Fig. 10. Deflection at small z grows quadratically with z, as geometrical optics predicts. At 1.8 km, the deflection curve show a rather severe change in slope. This appears to be due to a rapidly changing shape in the profile and to the fact that the beam is sampled a finite number of times.

Beam deflection, measured in the above fashion, is a crude measure of the location of the beam. It is quite conceivable that, with the growth of diffraction peaks along the line of symmetry, the deflection itself can show an abrupt discontinuity while the beam configuration is changing in a smooth and continuous fashion. Therefore the position of the peak intensity point along the central line indicates the beam displacement in a qualitative sense only.
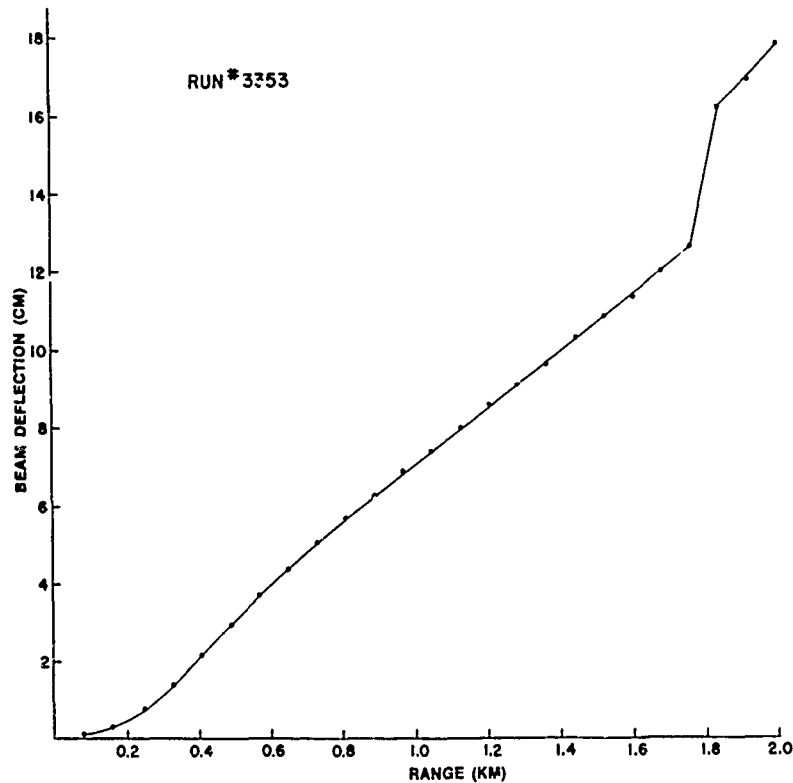
Fig. 10 – Beam deflection vs downrange distance for Run No. 3353.

The value of the peak intensity along the line of symmetry in a cross section of the beam is plotted vs range z, in Fig. 11. The peak intensity is seen to reach a maximum at 1.2 km. The decrease thereafter is related directly to the divergence of the beam.

The isoirradiance contours of Run #1155 are shown in Fig. 12. At $z = 1$ km, $\delta E/E = 1 \times 10^{-3}$ and the RQF is EXCELLENT. The sharp corners of the interior contours can be eliminated by using a finer mesh. Slewing and kinetic cooling are present. At a range of 1 km, $v_0 \tau = 30$ cm, while the beam size is reduced to about 6 to 10 cm in diameter. Thus, even with a large amount of water vapor present, the air is swept out of the beam before the excited nitrogen molecules decay to add to the heating, reducing the overall heating effect by .6. The high slewing rate further diminishes the heating. Although the calculation was not carried further, it is clear that diffraction will cause the beam to spread at larger ranges.

Beam deflections were less than 1 cm at all ranges up to 1 km in this run.

Plotted in Fig. 13 are the isoirradiance contours at the focal point for runs which have identical parameters, except water vapor pressure, to demonstrate the effect on a focused beam of the kinetic cooling phenomenon. All figures are drawn to the same scale. An absolute scale is shown below the left-most figure. The peak intensities, from left to right, are 3140 watts/cm^2, 490 watts/cm^2, and 640 watts/cm^2. The peak intensity value for the central figure is lower than that of the right one because of the development of two strong maxima in the beam. In contrast, the $1/e$ radius of a diffraction-limited beam (shown as a dashed circle centered on the beam axis, indicated by a small cross) is 1.65 cm, with a peak intensity of 11,250 watts/cm^2.
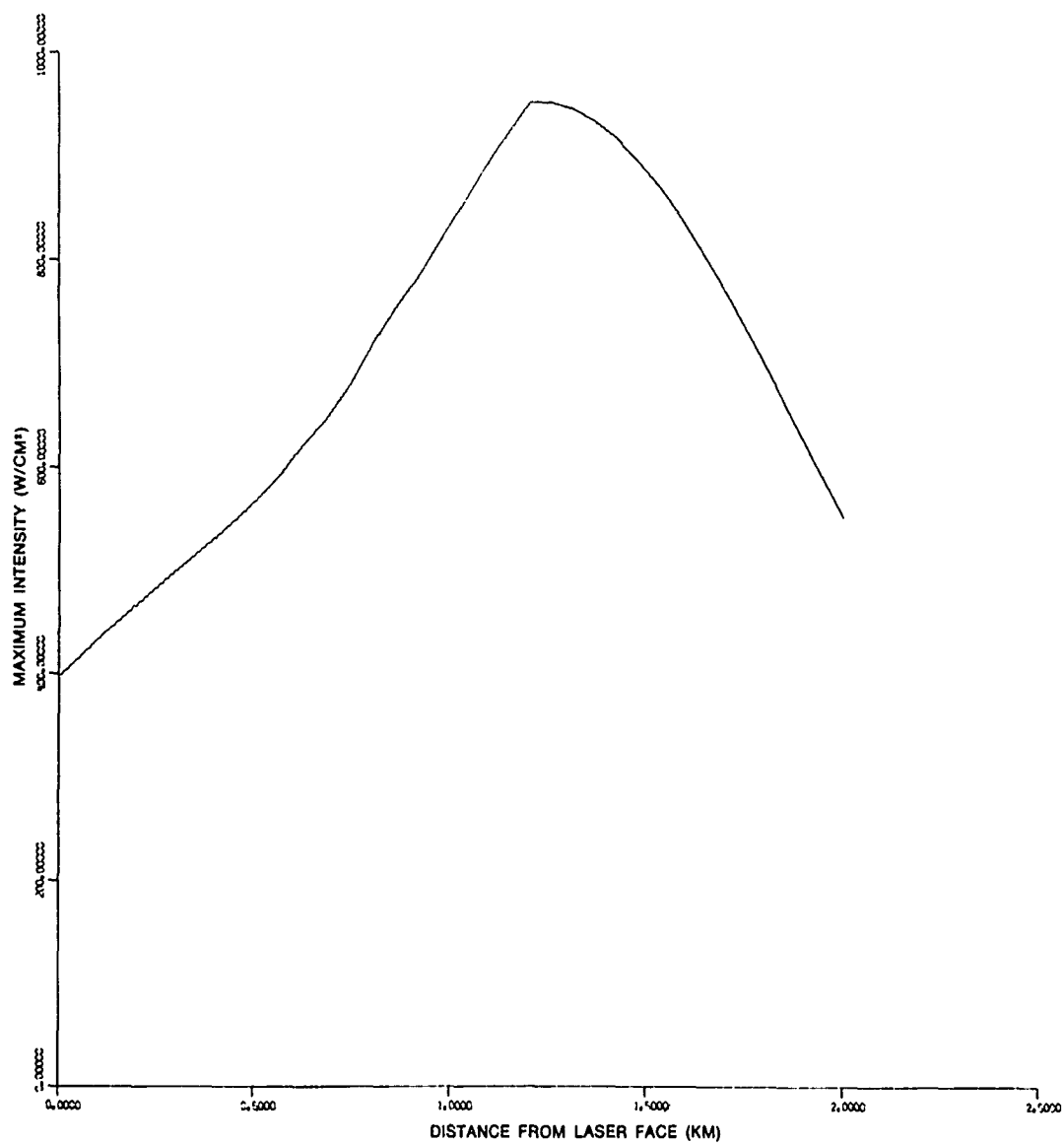
AITKEN, HAYES, AND ULRICH

Fig. 11 – Peak intensity in beam vs downrange distance for Run No. 3353.

Z= 0.5476

Z= 1.3615

Z= 0.2763

Z= 1.0902

Z= 0.0050

Z= 0.8189

RUN # 1155; (ACCEPTABLE); P = 10^5 watts; v_∞ = 200 cm/sec; a = 10 cm; (21,41); Ω = 0.15 rad/sec; f = 1 km; $\mathcal{L}$ = 3 km; $p(H_2O)$ = 12 Torr.; α = 2.26 $\times$ 10^{-6} cm^{-1}.

Fig. 12 – Run No. 1155.

AITKEN, HAYES, AND ULRICH

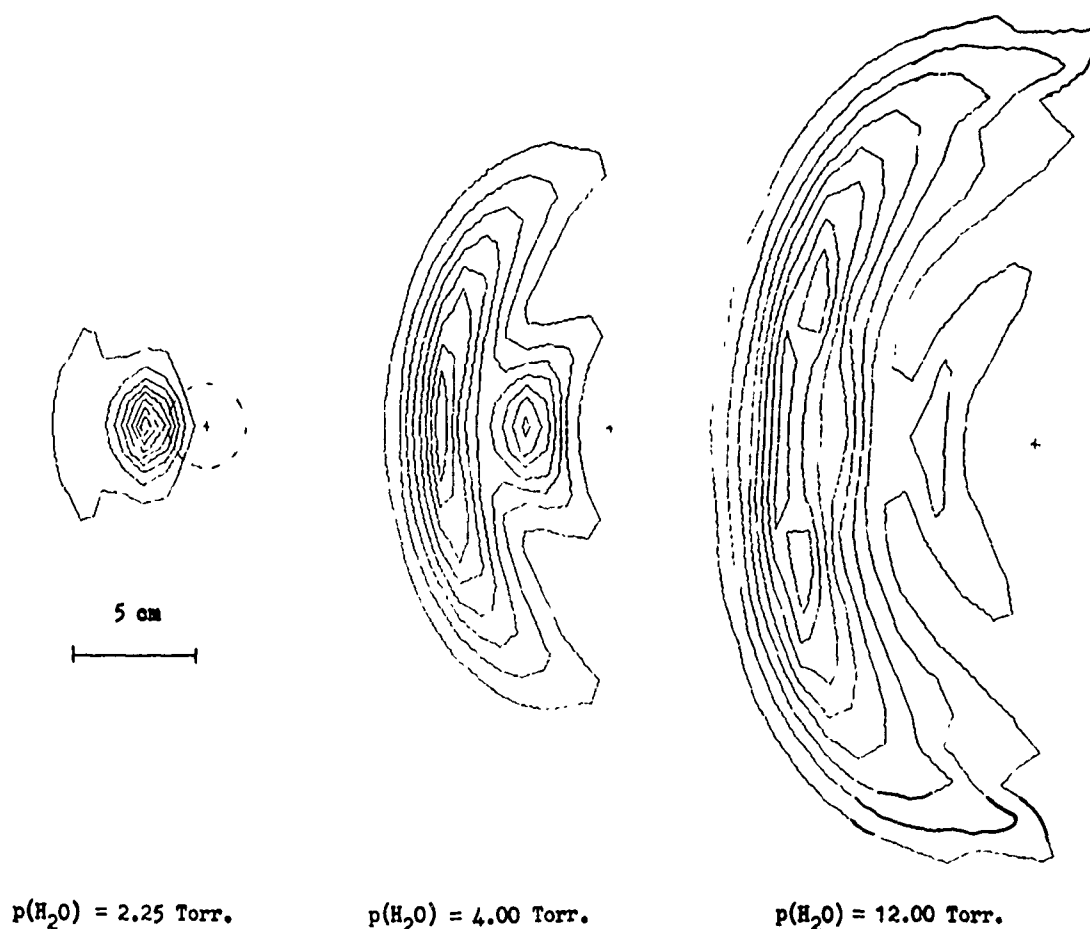p(H_2O) = 2.25 Torr.   p(H_2O) = 4.00 Torr.   p(H_2O) = 12.00 Torr.
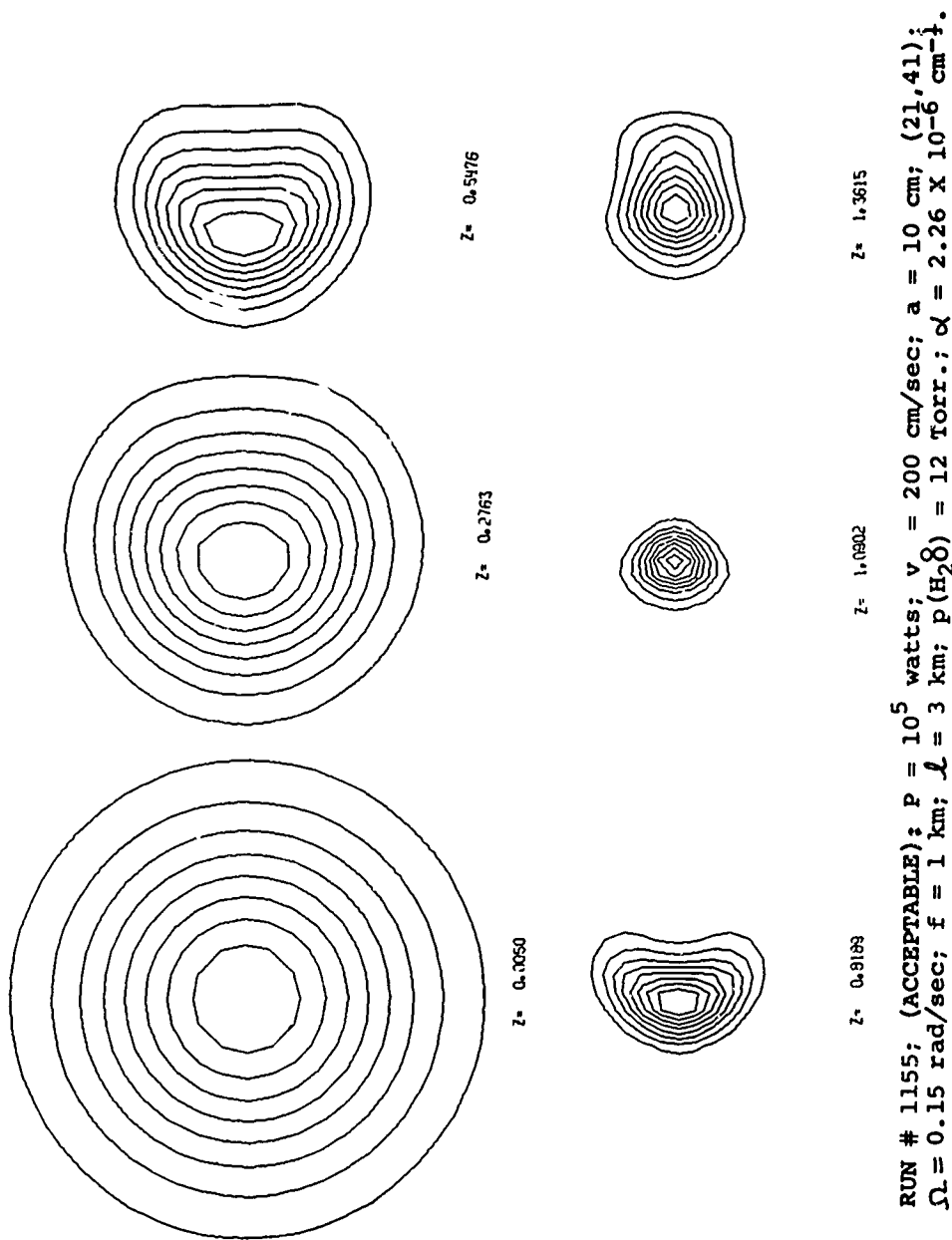
Fig. 13 - Comparison of the effects of water vapor pressure p (H_2O) on a focused beam.

The parameters that characterize the above runs, apart from water vapor, are
$P = 10^5$ watts; $a = 10$ cm; $v_0 = 200$ cm/sec; $\Omega = 0.00$ rad/sec; $f = 1$ km; and $(N_x, N_y) = (31, 61)$.

Run #3145, whose contours are shown in Fig. 14, was chosen with parameters to match the run reported by Wallace and Camac (11), who studied laser propagation using geometrical optics. They presented their contour plot at $z = .6$ km. The two figures, with the different normalizations accounted for, are in detailed agreement. Beyond this point, at 798 km, the beam, which was initially *collimated,* is undergoing *self-focusing.* (At $z = 798$ m, $\Delta E/E = 3 \times 10^{-4}$ and RQF is EXCELLENT.) The next figure can only be regarded as a qualitative representation of the phenomenon because the beam is collapsing to too small a configuration to be handled by the mesh size used in the computation.

ACKNOWLEDGMENTS

$l = 0.4019$ KM

$l = 0.2035$ KM

$l = 0.1050$ KM

$l = 0.9973$ KM

$l = 0.7999$ KM

$l = 0.6064$ KM

RUN # 3145; P = 3.90 X 10^5 watts; vo = 600 cm/sec; a = 10 cm;
Ω = 0.0 rad/sec; f = ∞; $\mathcal{L}$ = ∞; δ = 2.44; α = 6.7 X 10^{-7}cm^{-1}
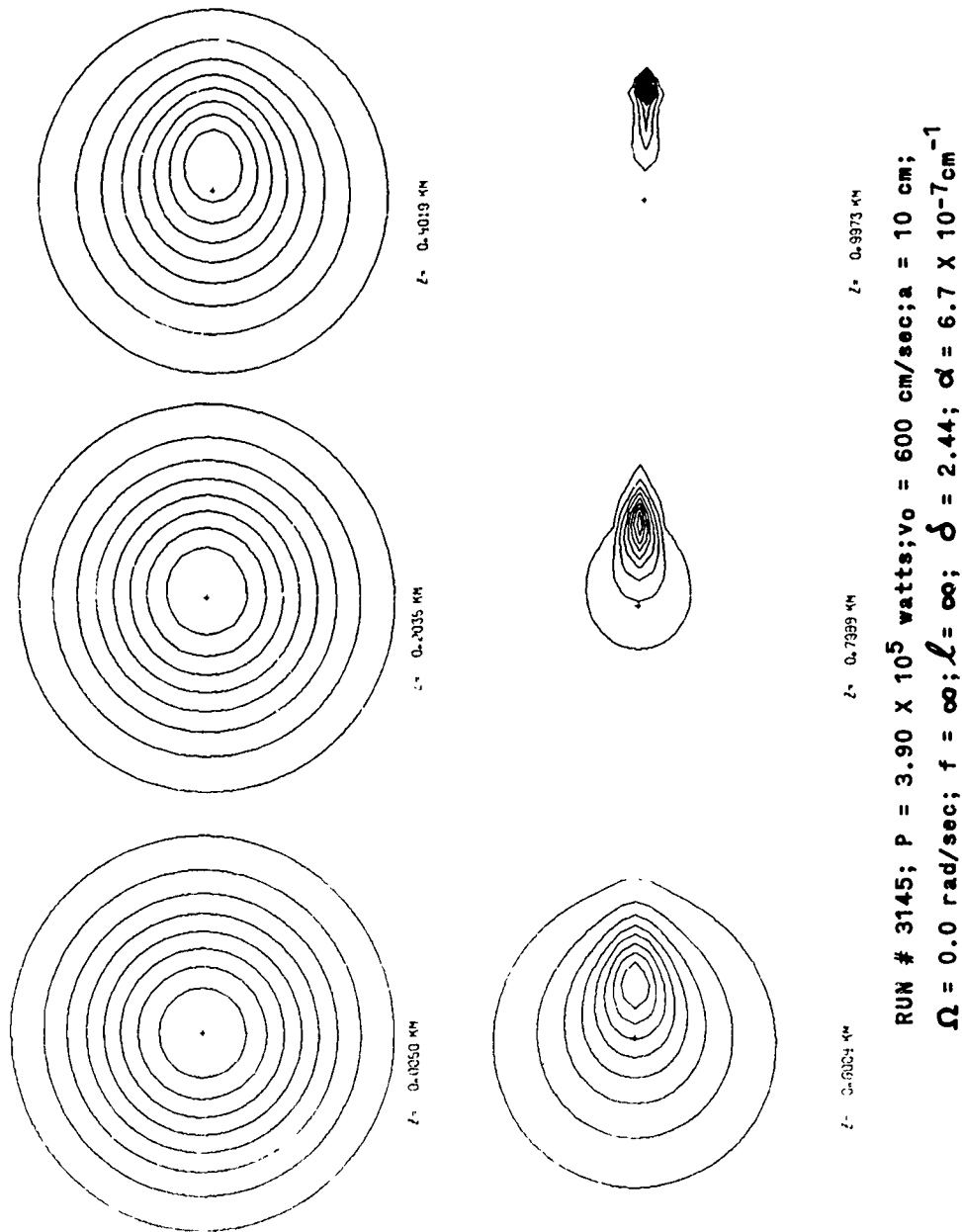
Fig. 14 – Run No. 3145: isoirradiance plots for a collimated beam. Results should be compared with the geometric optics results of Wallace and Comac (5).

REFERENCES

1. Gordon, J.P., Leite, R.C.C., Moore, R.S., Porto, S.P.S., and Whinnery, J.R., J. Appl. Phys. Phys., 36:3-8 (1965)

2. Leite, R.C.C., Moore, R.S., and Whinnery, J.R., Appl. Phys. Letters, 5:141-143 (1964)

3. Rieckhoff, K.F., Appl. Phys. Letters, 9:87-88 (1966)

4. Callen, W.R., Huth, B.G., and Pantell, R.H., Appl. Phys. Letters, 11:103-105 (1967)

5. Carman, R.L., and Kelley, P.L., Appl. Phys. Letters, 12:241-243 (1968)

6. Akhmanov, S.A., Krindach, D.P., Migulin, A.V., Sukhorukov, A.P., and Khokhlov, R.V., IEEE J. Quant. Elect., QE-4:568-575 (1968)

7. Hayes, J.N., "Thermal Blooming of Laser Beams in Gases," NRL Report 7213, Feb. 1971

8. Wagner, W.G., Univ. of Southern Calif., Electronic Sciences Laboratory Report 400, Oct. 1970. (Under certain conditions, steady states may not evolve.)

9. Gebhardt, F.G., and Smith, D.C., Appl. Phys. Letters 14:52-54 (1969)

10. Wood, A., Camac, M., and Gerry, E., Avco-Everett Research Laboratory Report 350, June 1970

11. Wallace, J., Jr., and Camac, E.M., JOSA, 60:1587 (1970)

12. Taylor, R.L., and Bitterman, S., Rev. Mod. Phys., 41:26 (1969)

13. Stephenson, J.C., Haseltine, W.A., and Moore, C.B., Appl. Phys. Letters, 11:164 (1967)

14. McCoy, J.H., Rensch, D.B., and Long, R.K., Appl. Opt., 8:1471 (1969)

15. Harmuth, H.F., J. Math. & Phys., 36:269 (1957)

16. Forsythe, G.E., and Wasow, W.R., "Finite Difference Methods for Partial Differential Equation," New York:Wiley and Sons, pp. 194 ff., 1960

17. Godanov, S., and Ryabenki, V., "Theory of Difference Schemes," North-Holland, Amsterdam: 1964, pp. 21 ff

18. Hamming, R.W., "Numerical Methods for Scientists and Engineers," New York: McGraw-Hill, pp. 115 ff., 1962

19. Wallace, J., Jr. (private communication)

Appendix A

FOCUSED COORDINATES

In numerical computation of solutions to Eq. (56), sufficiently small mesh sizes to describe the oscillations of the amplitude in the transferse directions are imperative. If, for focused beams, a fixed transverse mesh is used, there may be insufficient sampling in the vicinity of the focal region, especially for short focal lengths where the spot size, in vacuum at least, is certainly small. Variable mesh sizes may be achieved by using angular coordinates on concentric spherical surfaces as follows:

As was done in Section III, construct a right-handed coordinate system whose origin is at the center of the laser face, whose plane lies in the xy plane, and whose z axis is the direction of propagation. Downbeam a distance ℓ place the origin of a second right-handed coordinate system, with its z' axis pointing back towards the laser (see Fig. A1).
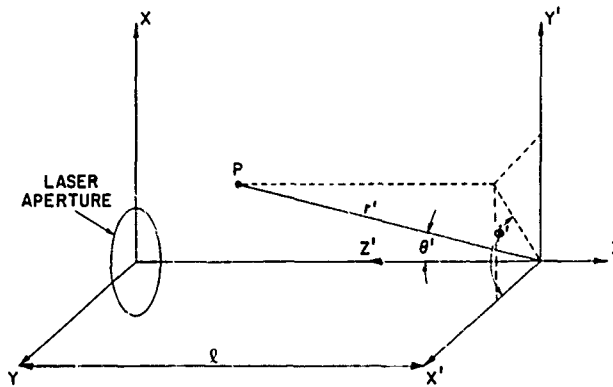

Fig. A1 - Relationship between three coordinate systems used in the discussion of focused coordinates.

With respect to this system construct the customary spherical polar coordinates; the coordinates of a point P in space will thus be characterized by (x, y, z) or by (r', θ', φ'). The Helmholtz equation in terms of the latter variables is

$$\frac{1}{(r')^2} \frac{\partial}{\partial r'} (r')^2 \frac{\partial \psi}{\partial r'} + \frac{1}{(r')^2 \sin \theta} \frac{\partial}{\partial \theta'} \sin \theta' \frac{\partial \psi}{\partial \theta'} + \frac{1}{(r')^2 \sin^2 \theta'} \frac{\partial^2 \psi}{\partial (\varphi')^2} + k^2 \epsilon \psi = 0 . \quad \text{(A1)}$$

For a wave propagating along the positive z direction we put

$$\psi(r', \theta', \varphi') = \frac{e^{-i \kappa r' - \frac{\alpha \ell}{2}}}{r'} \Phi(r', \theta', \varphi') , \quad \text{(A2)}$$

35

where

$$\kappa = k\epsilon_0^{1/2} + i\alpha/2 .$$

into Eq. (A1) and derive an equation for Φ which will involve $\partial^2\Phi/\partial(r')^2$ and $k\,\partial\Phi/\partial r'$. Dropping the second space derivatives as was done in the derivation of Eq. (1) and carrying only lowest order terms in the absorption coefficient, the equation for Φ becomes

$$-2ik\epsilon_0^{1/2} \frac{\partial\Phi}{\partial r'} + \frac{1}{(r')^2}\left[\frac{1}{\sin\theta'}\frac{\partial}{\partial\theta'}\sin\theta'\frac{\partial\Phi}{\partial\theta'} + \frac{1}{\sin^2\theta'}\frac{\partial^2\Phi}{\partial(\varphi')^2}\right]$$
$$+ k^2(\epsilon^{(r)} - \epsilon_0^{(r)})\,\Phi = 0 . \tag{A3}$$

At points between the focal point f of the beam and the laser face, the amplitude Φ will usually be small for all but small values of θ'. Carrying only the lowest orders of θ', Eq. (A3) is closely approximated by

$$-2ik\epsilon_0^{1/2} \frac{\partial\Phi}{\partial r'} + \frac{1}{(r')^2}\left[\frac{1}{\theta'}\frac{\partial}{\partial\theta'}\left(\theta'\frac{\partial\Phi}{\partial\theta'}\right) + \frac{1}{(\theta')^2}\frac{\partial^2\Phi}{\partial(\varphi')^2}\right]$$
$$+ k^2(\epsilon^{(r)} - \epsilon_0^{(r)})\,\Phi = 0 . \tag{A4}$$

A coordinate transformation

$$\hat{x} = \theta'\cos\varphi' , \qquad \hat{y} = \theta'\sin\varphi' \tag{A5}$$

converts Eq. (A4) into

$$-2ik\epsilon_0^{1/2} \frac{\partial\Phi}{\partial r'} + \frac{1}{(r')^2}\left(\frac{\partial^2\Phi}{\partial\hat{x}^2} + \frac{\partial^2\Phi}{\partial\hat{y}^2}\right) + k^2(\epsilon^{(r)} - \epsilon_0^{(r)})\Phi = 0 \tag{A6}$$

which is quite similar in form to Eq. (1). The quantities $\hat{x}$, and $\hat{y}$ are angular coordinates on spheres of radius r' in the transverse directions, as seen from the origin of the primed coordinate system.

If a is a characteristic transverse linear dimension (say beam radius) characterizing the initial laser beam profile, then $\theta_0 = a/\ell$ is a corresponding characteristic angular dimension. Scaling the variable $\hat{x}$ and $\hat{y}$ with this quantity, a new pair of variables $\bar{x}$ and $\bar{y}$ are introduced:

$$\bar{x} = \frac{\ell}{a}\hat{x} , \qquad \bar{y} = \frac{\ell}{a}\hat{y} . \tag{A7}$$

For those points in space where the amplitude is significantly different from zero, the variable r' may be related to the propagation distance z, to lowest order in θ', by

$$r' = \ell - z$$

and z is related to ζ by Eq. (53). In terms of the variables $\bar{x}$, $\bar{y}$, and ζ, Eq. (A6) becomes

$$2i \frac{\partial \Phi}{\partial \zeta} + \frac{1}{\left(1 - \frac{ka^2\zeta}{\ell}\right)^2} \nabla_1{}^2 \Phi + k^2 a^2 (\epsilon^{(r)} - \epsilon_0^{(r)}) \ \Phi = 0 \tag{A8}$$

while the intensity I now takes the form

$$I = \frac{P}{\pi a^2} \ e^{-ka^2\alpha\zeta} \ \frac{\Phi^*\Phi}{(1 - ka^2\zeta/\ell)^2} \ . \tag{A9}$$

The index of refraction is related to the amplitude Φ by

$$k^2 a^2 \ (\epsilon^{(r)} - \epsilon_0^{(r)}) = \frac{\beta e^{-ka^2\alpha\zeta}}{\left(1 - \frac{ka^2\zeta}{\ell}\right)} \int_{+\infty}^{\bar{x}} d\xi \left(1 - \delta e^{-\frac{n}{v_0\tau}\left(1 - \frac{ka^2\zeta}{\ell}\right)(\xi - \bar{x})}\right) |\Phi|^2 \ . \tag{A10}$$

The variables $\bar{x}$, $\bar{y}$, and ζ may be related to the original variables x, y, and z by

$$x = \left(1 - \frac{z}{\ell}\right) a\bar{y} \ , \qquad y = \left(1 - \frac{z}{\ell}\right) a\bar{x} \ , \qquad z = ka^2\zeta \ . \tag{A11}$$

In the limit that $\ell \longrightarrow \infty$, all previous results are recovered.

The solution to the boundary value problem posed by the differential equation [Eq. (A9)] requires the specification of the function on the spherical surface that goes through the point $x = y = z = 0$. On such a surface, the amplitude of a Gaussian beam focused at a distance f is given by

$$\frac{1}{\sqrt{\pi}} \ e^{-\rho^2/\rho_0^2} \ e^{ik\ell^2\left(\frac{1}{\ell} - \frac{1}{f}\right)\rho^2} \tag{A12}$$

To describe the oscillations in the real and imaginary parts of the amplitude that are due to the last factor in Eq. (A12), a transverse mesh size of appropriately small dimensions must be chosen. The larger the beam dimensions, the smaller this mesh size must be; the mesh size will also be correlated with the f ratio of the beam. For values of ℓ near f, such oscillations can be reduced considerably; for $\ell = f$, they vanish. If one is not interested in the behaviour of the beam as far as the focal point, this latter choice of ℓ is the appropriate one. Larger values of ℓ are required to study the beam in the vicinity of the focal length, since the denominators of the second and third terms (see Eq. (A10)) in the wave equation (Eq. (A8)) vanish at $z = \ell$, and the approximations on which the equation was based are no longer valid.

The numerical value of the quantity ℓ is determined by the problem itself. It is convenient, in practice, to attempt a numerical solution with fixed mesh size. If the results show a strong focusing of the beam, the numerical results can be made more reliable by redoing the computation with ℓ chosen slightly larger than the focal length. If the heating causes severe blooming in spite of the initial focusing, it may prove necessary to use a negative value of ℓ so that the coordinates are defocusing.

An alternative derivation of Eq. (A9), which is much simpler than the above but has less immediate geometrical significance, is obtained by putting

AITKEN, HAYES, AND ULRICH

$$\tilde{x} = \frac{1}{1 - ka^2\zeta/\ell}\, \bar{x} \quad \text{and} \quad \tilde{y} = \frac{1}{1 - ka^2\zeta/\ell}\, \bar{y} \quad , \tag{A13}$$

so that

$$\tilde{f}(\tilde{x}, \tilde{y}, \zeta) = f(\bar{x}(\tilde{x}, \zeta),\ \bar{y}(\tilde{y}, \zeta),\ \zeta) \tag{A14}$$

g.ving the equation

$$2i\, \frac{\partial \tilde{f}}{\partial \zeta} + 2i\, \frac{1}{1 - ka^2\zeta/\ell}\left(\tilde{x}\, \frac{\partial \tilde{f}}{\partial \tilde{x}} + \tilde{y}\, \frac{\partial \tilde{f}}{\partial \tilde{y}}\right) + \frac{1}{(1 - ka^2\zeta/\ell)^2}\, \tilde{\nabla}_\perp^2\, \tilde{f}$$

$$+\ k^2 a^2 (\epsilon - \epsilon_0)\, \tilde{f} = 0 \quad . \tag{A15}$$

The first-derivative terms are eliminated by defining a new amplitude φ by

$$\tilde{f} = \frac{\exp\left[-\,i\, \dfrac{ka^2}{2\ell}\left(1 - \dfrac{ka^2\zeta}{\ell}\right)(\tilde{x}^2 + \tilde{y}^2)\right]}{1 - ka^2\zeta/\ell}\, \varphi(\tilde{x}, \tilde{y}, \zeta) \quad . \tag{A16}$$

φ is then the amplitude in Eqs. (A9)–(A11). The equivalence of the two derivations is clear.

Appendix B

ANALYTICAL RESULTS

The computer code can be checked, in part, by comparing computer solutions of known problems with analytical results. The analytical results presented here provide a check on two different aspects of the code.

Vacuum Propagation

The vacuum propagation of a laser beam is described by Eq. (1) with β set equal to zero. The solution of the resultant equation is

$$\varphi(\vec{\rho}, z) = -\frac{i}{2\pi}\frac{k}{z} \iint dx' dy' \; \varphi(\vec{\rho}', 0) \; \exp\left(\frac{ik(\vec{\rho} - \vec{\rho}')^2}{2z}\right) . \tag{B1}$$

The integration is carried over the plane $z = 0$, and $\varphi(\vec{\rho}, 0)$ is the amplitude specified at the face of the laser. For a Gaussian beam whose power is normalized to unity and whose intensity is reduced from its central value by a factor of e at a radial distance a, and which is focused at a distance f down the beam axis,

$$\varphi(\vec{\rho}, 0) = \frac{1}{\sqrt{\pi a^2}} \exp\left[-\frac{\bar{\rho}^2}{2} - i\frac{\bar{\rho}^2}{2\hat{f}}\right] \tag{B2}$$

and

$$\varphi(\vec{\rho}, \zeta) = \frac{-i/\sqrt{\pi a^2}}{\zeta - i(1 - \zeta/\hat{f})} \; \exp\left[-\frac{\bar{\rho}^2}{2[\zeta^2 + (1 - \zeta/\hat{f})^2]} + i\frac{\bar{\rho}^2}{2\zeta}\left(1 - \frac{1 - \zeta/\hat{f}}{\zeta^2 + (1 - \zeta/\hat{f})^2}\right)\right] \tag{B3}$$

The intensity of the beam is given by

$$I(\vec{\rho}, z) = \frac{\exp[-\bar{\rho}^2/(\zeta^2 + (1 - \zeta/\hat{f})^2)]}{\pi a^2[\zeta^2 + (1 - \zeta/\hat{f})^2]} \tag{B4}$$

In Eqs. (B2), (B3), and (B4), $\bar{\rho}^2 = (x^2 + y^2)/a^2$, $\zeta = z/ka^2$, and $\hat{f} = f/ka^2$.

A collimated beam is obtained from the limit of infinite focal length:

$$\varphi_c(\vec{\rho}, 0) = \frac{1}{\sqrt{\pi a^2}} \exp\left[-\frac{\bar{\rho}^2}{2}\right] \tag{B5}$$

39

$$\Phi_c(\vec{\rho}, z) = \frac{-i}{\zeta - i} \frac{\exp\left[-\frac{\bar{\rho}^2}{2(1 + \zeta^2)} + i\,\frac{\bar{\rho}^2}{2}\,\frac{\zeta}{1 + \zeta^2}\right]}{\sqrt{\pi a^2}} \tag{B6}$$

$$I_c(\vec{\rho}, z) = \frac{\exp[-\bar{\rho}^2/(1 + \zeta^2)]}{\pi a^2(1 + \zeta^2)} \ . \tag{B7}$$

By comparing the numerically computed solutions for these cases with the analytical results, those portions of the code that deal with the linear parts of the equation are checked, and the linear stability and convergence of the algorithm can be ascertained.

High-Energy Beams

When the absorbed power in the central portions of the beam near the laser face is large, the nonlinear term in Eq. (56) will be much larger than the Laplacian term. Such a state of affairs is local only, since the opposite must hold in the wings of the beam. For this local region, however, Eq. (56) may be approximated by

$$2i\,\frac{\partial f}{\partial \zeta} - \beta e^{-ka^2\alpha\zeta}\,f\int_{-\infty}^{0} ds \left(1 - \delta e^{\frac{\alpha s}{v_0 \tau}}\right)|f|^2 = 0 \ . \tag{B8}$$

From Eq. (B8) and its complex conjugate, it may easily be shown that

$$\frac{\partial}{\partial \zeta}\,|f|^2 = 0 \tag{B9}$$

Hence the integral is independent of the variable ζ, and therefore Eq. (B8) may be integrated directly to give

$$f(\vec{\rho}, \zeta) = f(\vec{\rho}, 0)\,\exp\left[\frac{i\beta}{2}\left(\frac{e^{-ka^2\alpha\zeta} - 1}{ka^2\alpha}\right)\int_{-\infty}^{0} ds\left(1 - \delta e^{\frac{\alpha s}{v_0 \tau}}\right)|f(\vec{\rho} + s\hat{v}_0, 0)^2|\right] \ . \tag{B10}$$

Equation (B8) and its solution (B10) prove useful in two ways. Regardless of how good the approximation of dropping the Laplacian in any one specific case may prove to be, those portions of the computer code that deal specifically with the Laplacian may be bypassed, solving Eq. (B8) instead of Eq. (56). Thus, a check is provided on the formulation and accuracy of the code in treating the nonlinear portions alone. Also, for high values of γ, the oscillations of the amplitude as a function of ζ, induced by the heating, must be sampled at least six times per oscillation to be certain of accuracy. Dropping the cooling portion of the integral and using a Gaussian beam, this condition yields a restriction on stop size of

$$\gamma \Delta \zeta \leqslant 1 \tag{B11}$$

which was found, in practice, to be necessary indeed, as was discussed in Section IV.

Appendix C

EFFECTS OF THERMAL CONDUCTION

In this appendix, the size of the thermal conduction terms, which have not been included in the analysis, will be estimated, and their neglect justified. Thermal conductivity, which provides a mechanism for energy transfer in addition to the hydrodynamic motion, changes the energy conservation Eq. (7) to

$$\frac{dp_1}{dt} - \frac{\kappa}{\rho_0 c_v} \nabla^2 p_1 - c_s^2 \left(\frac{d\rho_1}{dt} - \frac{\kappa}{\rho_0 c_p} \nabla^2 \rho_1 \right) = (\gamma - 1) \rho_0 \dot{Q} \quad .$$

The effect of the added terms is estimated using the solution obtained by neglecting them. The pressure and its gradients are negligible in any case, so only the density terms are considered; replacing the ∇^2 term by derivatives along the wind where maximum changes occur, and ρQ by αI, the ratio of the conduction term to the transport term then is

$$\frac{(\kappa/\rho_0 c_p) \nabla^2 \rho_1}{v_0 \rho_1} = \frac{\kappa}{\rho_0 c_p v_0} \frac{1}{I} \frac{dI}{dx} \quad .$$

The factor $(1/I)(dI/dx)$ determines a characteristic inverse length appropriate to our estimate; this length can be estimated from the output intensity profiles at the smallest cross section of the beam and is about 1 cm in the most severe cases. Using the appropriate thermal constants for air, and for a wind speed of 200 cm/sec, the above ratio is of the order of 10^{-3}; when slewing is included, the ratio is even smaller. The effects of thermal conduction in the cases presented are negligible since this estimate provides only an upper limit to these effects; each case must, however, be considered separately.

41